AFGL-TR-87-0029

MHD Modeling of Energy Build-up Due to Photospheric Shearing Motion and Its Relation to Flare Prediction Criteria

S. T. Wu
J. B. Smith, Jr.

University of Alabama in Huntsville
Department of Mechanical Engineering
Huntsville, AL 35899

23 September 1987

Final Report
November 1982 - September 1985

Approved for public release; distribution unlimited

AIR FORCE GEOPHYSICS LABORATORY
AIR FORCE SYSTEMS COMMAND
UNITED STATES AIR FORCE
HANSCOM AIR FORCE BASE, MASSACHUSETTS 01731

This technical report has been reviewed and is approved for publication.

Donald F. Neidig
DONALD F. NEIDIG
Contract Manager

Stephen L. Keil
STEPHEN L. KEIL
Chief, Solar Research Branch

FOR THE COMMANDER

Rita C. Sagalyn
RITA C. SAGALYN, Director
Space Physics Division

This report has been reviewed by the ESD Public Affairs Office (PA) and is releasable to the National Technical Information Service (NTIS).

Qualified requestors may obtain additional copies from the Defense Technical Information Center. All others should apply to the National Technical Information Service.

If your address has changed, or if you wish to be removed from the mailing list, or if the addressee is no longer employed by your organization, please notify AFGL/DAA, Hanscom AFB, MA 01731. This will assist us in maintaining a current mailing list.

Do not return copies of this report unless contractual obligations or notices on a specific document requires that it be returned.

Unclassified
SECURITY CLASSIFICATION OF THIS PAGE

REPORT DOCUMENTATION PAGE

Form Approved OMB No. 0704-0188

1a. REPORT SECURITY CLASSIFICATION: Unclassified	1b. RESTRICTIVE MARKINGS
2a. SECURITY CLASSIFICATION AUTHORITY	3. DISTRIBUTION/AVAILABILITY OF REPORT: Approved for public release; Distribution unlimited.
2b. DECLASSIFICATION/DOWNGRADING SCHEDULE	
4. PERFORMING ORGANIZATION REPORT NUMBER(S)	5. MONITORING ORGANIZATION REPORT NUMBER(S): AFGL-TR-87-0029
6a. NAME OF PERFORMING ORGANIZATION: The University of Alabama in Huntsville; 6b. OFFICE SYMBOL (If applicable)	7a. NAME OF MONITORING ORGANIZATION: Air Force Geophysics Laboratory
6c. ADDRESS (City, State, and ZIP Code): Department of Mechancial Engineering, Huntsville, AL 35899	7b. ADDRESS (City, State, and ZIP Code): Hanscom AFB, Massachusetts 01731
8a. NAME OF FUNDING/SPONSORING ORGANIZATION; 8b. OFFICE SYMBOL (If applicable)	9. PROCUREMENT INSTRUMENT IDENTIFICATION NUMBER: F19628-83-K-0019
8c. ADDRESS (City, State, and ZIP Code)	10. SOURCE OF FUNDING NUMBERS: PROGRAM ELEMENT NO. 61102F; PROJECT NO. 2311; TASK NO. G3; WORK UNIT ACCESSION NO. CV

11. TITLE (Include Security Classification)
MHD Modeling of Energy Build-up Due to Photospheric Shearing Motion and Its Relation to Flare Prediction Criteria

12. PERSONAL AUTHOR(S)
S. T. Wu and J. B. Smith, Jr.*

13a. TYPE OF REPORT	13b. TIME COVERED	14. DATE OF REPORT (Year, Month, Day)	15. PAGE COUNT
Final Report	FROM 11/82 TO 9/85	1987 September 23	92

16. SUPPLEMENTARY NOTATION
*NOAA/SEL, Boulder, CO 80307

17. COSATI CODES		
FIELD	GROUP	SUB-GROUP

18. SUBJECT TERMS (Continue on reverse if necessary and identify by block number)
Energy storage in solar magnetic fields; Solar magnetohydrodynamics; Solar flares; Vector magnetic fields; Sheared magnetic fields.

19. ABSTRACT (Continue on reverse if necessary and identify by block number)

An investigation of the evolution of active regions, leading to the buildup and storage of magnetic energy for eventual rapid release as the thermal, radiative and kinetic energy of solar flares is presented. This investigation is based on both observations and theoretical models.

Solar observations utilized in the study were vector magnetograms, high-resolution hydrogen alpha filtergrams, flare data and sunspot pictures (for the energy buildup model). Active regions were selected on the basis of the availability of the appropriate observations, and the apparent potential for at least limited flaring. Parameters selected for the initial analysis, generally indicative of (available) magnetic energy buildup, include (1) the angle of shear, (2) the strength of the sheared field, (3) the longitudinal gradient (4) a parameter related to the shear volume, and in an observationally limited number of cases, (5) the vertical component of the current and (6) the MHD modeled energy buildup. In the limited data sample considered, significant flare production correlates well with indications of strong magnetic shear and energy storage. → next page

20. DISTRIBUTION/AVAILABILITY OF ABSTRACT: ☐ UNCLASSIFIED/UNLIMITED ☐ SAME AS RPT. ☐ DTIC USERS	21. ABSTRACT SECURITY CLASSIFICATION: Unclassified
22a. NAME OF RESPONSIBLE INDIVIDUAL: Donald Neidig	22b TELEPHONE (Include Area Code); 22c. OFFICE SYMBOL: AFGL/PHS

DD Form 1473, JUN 86 — Previous editions are obsolete. — SECURITY CLASSIFICATION OF THIS PAGE: Unclassified

19. The theoretical models are based on magnetohydrodynamic (MHD) theory. Specifically, a two-dimensional, non-planar, time-dependent MHD model was used to deduce the cirtical parameters as eventual input to a proposed "shear/flare index". However, these theoretically deduced physical parameters have to date had only limited comparison with observations.
In conclusion, we may state that this combined theoretical and observational study could lead to the development and refinement of a "magnetic shear/flare index" for the improvement of solar flare prediction technology.

SUMMARY

An investigation of the evolution of active regions, leading to the buildup and storage of magnetic energy for eventual rapid release as the thermal, radiative, and kinetic energy of solar flares, is presented. This investigation is based on both observations and theoretical models.

Solar observations utilized in the study were vector magnetograms, high-resolution Hydrogen-Alpha filtergrams, flare data, and sunspot pictures (for the energy buildup model). Active regions were selected on the basis of the availability of the appropriate observations, and the apparent potential for at least limited flaring. Parameters selected for the initial analysis, generally indicative of (available) magnetic energy buildup, include (1) the angle of shear, (2) the strength of the sheared field, (3) the longitudinal gradient, (4) a parameter related to the sheared volume, and, in an observationally limited number of cases, (5) the vertical component of the current and, (6) the MHD modeled energy buildup. In the limited data sample considered, significant flare production correlates well with indications of strong magnetic shear and energy storage.

The theoretical models are based on magnetohydrodynamic (MHD) theory. Specifically, a two-dimensional, non-planar, time-dependent MHD model (i.e., usually called two- and one-half-dimensional, time-dependent, MHD model in which both velocity and magnetic fields have three components but the spatial dependence is two-dimension) was used to deduce the critical parameters as eventual input to a proposed "shear/flare index". However, these

theoretically deduced physical parameters have to date had only limited comparison with observations.

In conclusion, we may state that this combined theoretical and observational study could lead to the development and refinement of a "magnetic shear/flare index" for the improvement of solar flare prediction technology.

TABLE OF CONTENTS

I. INTRODUCTION

The operation of military, as well as civilian, satellites and systems for communications, tracking, and surveillance can be interrupted, degraded, or even endangered as a result of powerful, impulsively energetic, "explosive" phenomena on the surface of the sun, called solar flares. These spectacular eruptions release shock waves, hot plasma clouds, highly accelerated atomic nuclei, and bursts of x-rays, ultraviolet, radio, and visible-band electromagnetic radiation into inter-planetary space (e.g. Svestka, 1976). When the path of propagation of the high-energy mass ejecta intersects the earth's magnetosphere, our terrestrial environment is impacted in various ways that may produce deleterious effects on systems both on the ground and in space. Thus, the technology development for improved methods of solar flare prediction is imperative in this technological era. Toward achieving this goal, the first step is the understanding of the fundamental physical processes and developing the characteristic parameters of the solar flare.

In this report, we shall address such a scenario, based on both the observational and the theoretical modeling approach. Recently, it has been shown that photospheric shear has been well

correlated with the occurrence of solar flares (Smith, et al., 1984; Hagyard et al., 1984). de Loach et al. (1984) found that the photospheric electric currents, deduced from the observed photospheric (vector) magnetic fields, were correlated with the transition region brightness as observed in ultraviolet spectroheliograms, obtained by the UVSP experiment on board the Solar Maximum Mission satellite. Hagyard et al. (1986) also tentatively established the critical shear angle in relation to the occurrence of major solar flares (based on a small sample). Theoretically, it has also been shown that the photospheric shear motion is the primary candidate as a physical mechanism for the flare energy build-up (Wu et al., 1984), and the joule dissipation can be considered as the physical mechanism for flare energy release (Wu et. al 1986). These observational and theoretical results indicate a possibility for developing a quantity (a shear index) which can be used in the determination of an active region's potential for major flare production, such that it may lead to improved flare prediction techniques.

In this report, we shall first (in selected appropriate cases, where required spot observations were available) establish from observations the photospheric shear motion in relation to flare occurrence. We shall then use the magnetohydrodynamic (MHD) model to quantize some physical parameter which will be verified by observations. In Chapter II, the data analysis is discussed, including the method of data selection, a description of the data, and some preliminary correlative analysis (toward development and testing of a shear index). Finally, we summarize

the general characteristics shown from these data. The theoretical modeling effort is presented in Chapter III, which includes magnetohydrodynamic (MHD) theory, numerical results, and physical interpretation of these obtained numerical results. Finally, the concluding remarks are presented in Chapter IV.

II. DATA ANALYSIS

The study was undertaken to determine if analysis of magnetic shear (and shearing motion) yields a promising predictor of the magnitude and frequency of solar flares from an active region. Additionally, in the case of the energy build-up model, can shear build-up can be usefully extrapolated into the future, and used as an indicator of flare specifics or of changing activity levels? The data selection and methodology of initial data analyses were determined by (1) the input parameters required in the physical model calculations and (2) the parameters selected for the empirical study of evidence of energy storage and its correlation with active region flare production.

1. Selection of Data

Intervals and Solar Active Regions were selected for analysis entirely on the basis of the availability of an adequate data set for a candidate active region. The adequacy of the data set was partially dependent on the type of analysis to be done but, in all cases, it was considered necessary that photospheric vector magnetic field data (Marshall Space Flight Center data) be available for the period of analysis. Chromospheric structure (as observed in high resolution Hydrogen Alpha) also yields valuable information on the orientation of the transverse

component of the magnetic field at the chromospheric level, but this information is qualitative and based somewhat on interpretation. Therefore, frequent high-resolution hydrogen-alpha photographs were considered important, but not always essential to the analysis. Dependable flare observations are required, and high quality observations and reports (occurrence, magnitude, and time profiles) were usually available from the AWS/SOON solar optical observing network. These were supplemented by reports from other observatories of the NOAA/AWS real-time network and contributors to the Solar Geophysical Data Center activity summaries.

2. Description of Data

Solar magnetic field data were NASA/Marshall Space Flight Center (MSFC) vector magnetograms, supplemented by line-of-sight magnetograms from other sources, such as the Kitt Peak National Observatory and the SOON system. Flare photographs and reports were obtained from the real-time NOAA/AWS system (mostly SOON optical data and NOAA GOES x-ray data). Imaged H-alpha and sunspot data from various sources, primarily the AWS/SOON system supplemented by NOAA and other observatories, were utilized in the study and are discussed below.

2.1 Data Types, Availability

The MSFC vector magnetograms, yielding both the line-of-sight and transverse components of the photospheric magnetic field, were the primary input data required for the initial qualitative analysis and flare correlation study. (The data, data acquisition methodology, and analysis techniques are

described elsewhere. See, for example, Hagyard, et al., 1982, Krall, et. al., 1982 and West and Hagyard, 1983). From these data, the observable parameters considered indicative of active region energy storage (angle of shear, an estimate of the affected volume, the field strength, and the gradient of the longitudinal component of the field) were measured or implied. The AF/AWS SOON acquired high spatial resolution H-alpha, intermittently available for the analyzed active regions, were used to imply the direction of the transverse component of the chromospheric magnetic field. Although the analysis concentrates primarily on the quantitative, objective information contained in the vector magnetograms, we compared this observed transverse photospheric magnetic field orientation with chromospheric fibril orientation in the major flare producing active regions. (This comparison has tended to validate the potential for application, in appropriate cases, of high resolution H-alpha observations to operational shear analysis. Comparison may also offer insight into the vertical structure of the magnetic field in the lower solar atmosphere.) Sunspot observations with the necessary temporal and spatial resolution required for sunspot proper motion analysis were usually not available. Some very high quality white-light observations made by the Sacramento Peak National Solar Observatory were used in the analysis of one exceedingly important 1980 active region (see Neidig et al., 1986). Air Weather Service SOON observatories, with their high-resolution off-band H-alpha filtergrams, were also an important source for sunspot observations. Correlative flare information

was acquired primarily from the NOAA preliminary reports of solar and geophysical data, issued weekly and incorporating the AWS/SOON solar event reports as their primary data source.

2.2 1980 Multiple Regions

During the Solar Maximum Mission (SMM), launched early in 1980 and with an initial concentrated observational period lasting through most of 1980, the MSFC solar observatory acquired correlative vector magnetograms during all acceptable observing periods. Other solar observatories, including the AWS/SOON real-time observatory network, also concentrated on SMM observing targets during this interval. Therefore, many of the interesting solar active regions (ARs) of this active period in the solar cycle were well observed and therefore appropriate for analysis.

2.3 Post-1980 Active Regions

Soon after the temporary termination of the imaged SMM observations late in 1980, the MSFC vector magnetograph interrupted observations for a prolonged period of major maintenance and system upgrading. Additionally, SOON observatories reduced their photographic high-resolution H-alpha observations to a "by exception" status. At the time of completion of the MSFC magnetograph modification, the sun had entered the very low level of solar activity characteristic of an approaching solar minimum. These factors have combined to severely limit the opportunities for additional active region analysis. With this very low general level of solar activity, we were fortunate in the appearance and development of two very interesting active regions. One (AR4711) an excellent candidate

TABLE II.1

SOLAR ACTIVITY - FEBRUARY 1986
ACTIVE REGION 4711

CLASS M AND X FLARES, AND PRINCIPLE GEOMAGNETIC RESPONSES

NO.	DATE (X-ray maximum)	LOCATION (Active Region #)	CLASSIFICATION (optical/x-ray)	RADIO BURSTS (meter/ sweep)	REMARKS
1	3 Feb (2049UT)	S09 E26 (4711)	1B/M2.3	Type II Type IV	- See SSC below (6th
2	02/04 (0741UT)	S03 E21 (4711)	3B/X3.0	Type II	
3	02/04 (1029UT)	S02 E68 (4713)	1B/M6.4	-	
4	02/05 (1255UT)	S07 E06 (4711)	2B/M3.0	-	
5	02/06 (0625UT)	S04 W06 (4711)	3B/X1.7	Type II Type IV	- GIOTTO measured shock from this flare on 8 Feb. (0230UT) at + ~0.72 AU, 53° west of Earth. - Same shock predicted at Earth: 8 Feb. (1322UT). - SSC (from flares # 1 and 2) at (1313UT).
6	02/07 (1034UT)	S10 W20 (4711)	2B/M5.2	Type IV	- Major geomagnetic storm began on 7 Feb. and reached maximum levels on 8 Feb. - Multiple shock arrivals (see above).

End of AR4711 major flares.

for analysis, appeared during early February, 1986, exhibited growth, and produced significant flares. (The significant flares and related terrestrial events associated with this region are listed in Table II.1.) Several interesting areas developed in the active region, and analysis is somewhat limited by the time resolution of the data (weather frequently interfered with vector magnetogram acquisition). Flare observations were generally good, and the site of flare onset, as unambiguously determined (from photographs), is presently known for some of the flares.

Limited analysis has also been initiated on several generally small and simple active regions, with no appropriate results for reporting here.

3. Summary of General Characteristics

Logically, the determination of the presence (and buildup) of energy stored in a sheared, non-potential magnetic field- energy available for conversion to the thermal, radiative, and kinetic energy released during solar flares - should lead to improved flare predictive techniques. In fact, in this continuing study of the correlation of magnetic shear with flare occurrence, we have found a distinct preference for high flare productivity and, particularly, of major flares for areas with observational evidence of significant magnetic shear. Striking examples are in areas of increasing shear, clearly accompanied by an increase in flare magnitude and frequency.

Analysis has yielded several measurable parameters for test correlations with flare production. These include:

a. The maximum "angle of shear", determined by comparing the direction of the observed transverse component with that of the potential field direction, either calculated or estimated. This, along with field strength, is the primary observational parameter. Both have been found to be critical in defining major flare onset sites.

b. The field strength, averaged along the selected neutral line segment. Since the longitudinal component is zero along the neutral line, this is essentially the strength of the transverse component of the field.

c. The length of the affected neutral line segment. This is an easily measured quantity, related to the volume and hence to the total available energy. Length of the sheared neutral lines has also have been qualitatively related to major flare prediction, with implication of a minimum length requirement. Quantitative correlation of this parameter and of the B_L gradient should proceed.

d. B_L gradient, determined from longitudinal magnetograms. This quantity, averaged over the affected area, can be determined objectively and with analysis of spatial distribution, but is here (in Table II.2) stated stated qualitatively (but based on objective criteria).

e. The vertical component of the electric field, as calculated from the vector magnetic field. This quantity has only been analyzed for a limited number of cases, and will probably have limited application.

f. The (MHD model determined and dependent) calculated and extrapolated magnetic energy buildup is based on photospheric proper motions, determined from sunspot observations. The projected energy buildup is promising as a predictive parameter (Wu et al., 1984).

g. The complexity of the involved magnetic field offers promise, but has not yet been included in the analysis a in the tentative flare-prediction index.

h. Sunspot motion: Because of the sparsity of sunspot observations with adequate temporal and spatial resolution, the shearing motion of sunspots has not yet been tested as a separate parameter, but only as an input to the MHD modeling. However, this technique (model application) provides a parameter more directly applicable in energy analysis. Nevertheless, sunspot motion appears promising as a unique parameter, and will be tested in future case studies.

A "shear index" to be applied in operation time prediction, has been tentatiaavely defined, incorporating the observational parameters in Table II.2. Further refinement, developmental testing, and operational testing of the predictive index are planned. Objective determination of a related parameter will be difficult, but should include neutral line complexity and isolated poles, etc.

3.1 Discussion of Specific Regions

In 1980, near solar maximum and during the intensive solar observing period of the Solar Maximum Mission (SMM), we were

fortunate in having several appropriate regions for analysis (see Table II.2). Among these were two pairs of simultaneously visible regions; each region of observational interest and with apparent flare production potential. In each case, without detailed magnetic field analysis the regions appeared equally capable of flare production. But, again in each case, the regions with significant observable shear were flare productive, while those with essentially potential fields (or weak, somewhat sheared fields) were the source of only low levels of activity. The most striking and most analyzed pair, AR2372 (flare productive) and AR2370 (few small flares), occurred in April 1980.

AR2370, a large region with strong magnetic fields, rotated onto the visible disk with apparent potential for significant activity. However, vector magnetograms revealed that the magnetic field of AR2370 was near potential in configuration. In fact, AR2370 produced little activity of note. Soon after the appearance of AR2370, AR2372 emerged (early on the 4th of April 1980) as a simple, but rapidly growing, bipole just ahead and somewhat south of AR2370. Coalescence of small spots soon began (Ding You Ji, private communication), leading to the rapid formation of large leader and follower spots. Additional bipolar flux rapidly appeared with the emergence of a north-south oriented bipolar spot pair located just ahead and somewhat south of the large negative spot. (The subsequent evolution of longitudinal magnetic field (B_L) of AR2372 is shown in Figure II.1.) By early on the 5th, the enclosed positive polarity was

TABLE II.2

ACTIVE REGION SHEAR PARAMETERS AND FLARE OCCURRENCE

AR[1]	Shear[2]	* ℓ[3]	$\lvert\bar{B}\rvert$ (gauss)[4]	* $\frac{\Delta B_L}{\Delta s}$[5]	* Jz[6]	* Activity Level (qualitative)
2370	< 40°	---	---	moderate	+	flares (minor)
2372[a]	< 40°	long	500-1000	moderate	+	minor flare
2372[b]	70-90°	long	1000	strong	max	high activity level
2463	< 40°	short	< 500	weak	+	minor flares
2470[a]	30-60°	long	1000	moderate	+	moderate activity level
2470[b]	60-90°	short	1000	moderate	+	high activity level
2523	30-60°	short	< 500	+	+	numerous minor flares few small 'Ms'
2544	< 40°	short	< 500	+	+	rash of activity with an M1 ans an X2
2725	30-60°	medium	500-1000	+	minor	few Ms and an X3/3B
2776	60-90°	long	1000-1500	strong	max	major flare source numerous flares
4711	60-90°	mdt-long	1000	strong	+	major flare source numerous flares

[1] NOAA/Boulder (SESC) Active Region Number
[2] "Angle of Shear"; Difference from Potential Field Orientation
[3] Length of Involved Neutral Line
[4] Average Field Strength Along Involved Neutral Line
[5] Gradient of the Longitudinal Field Along Neutral Line
[6] Vertical Component of the Current as Calculated from the Transverse Component of the B Field
* Parameters to be Quantized
\+ Not Available

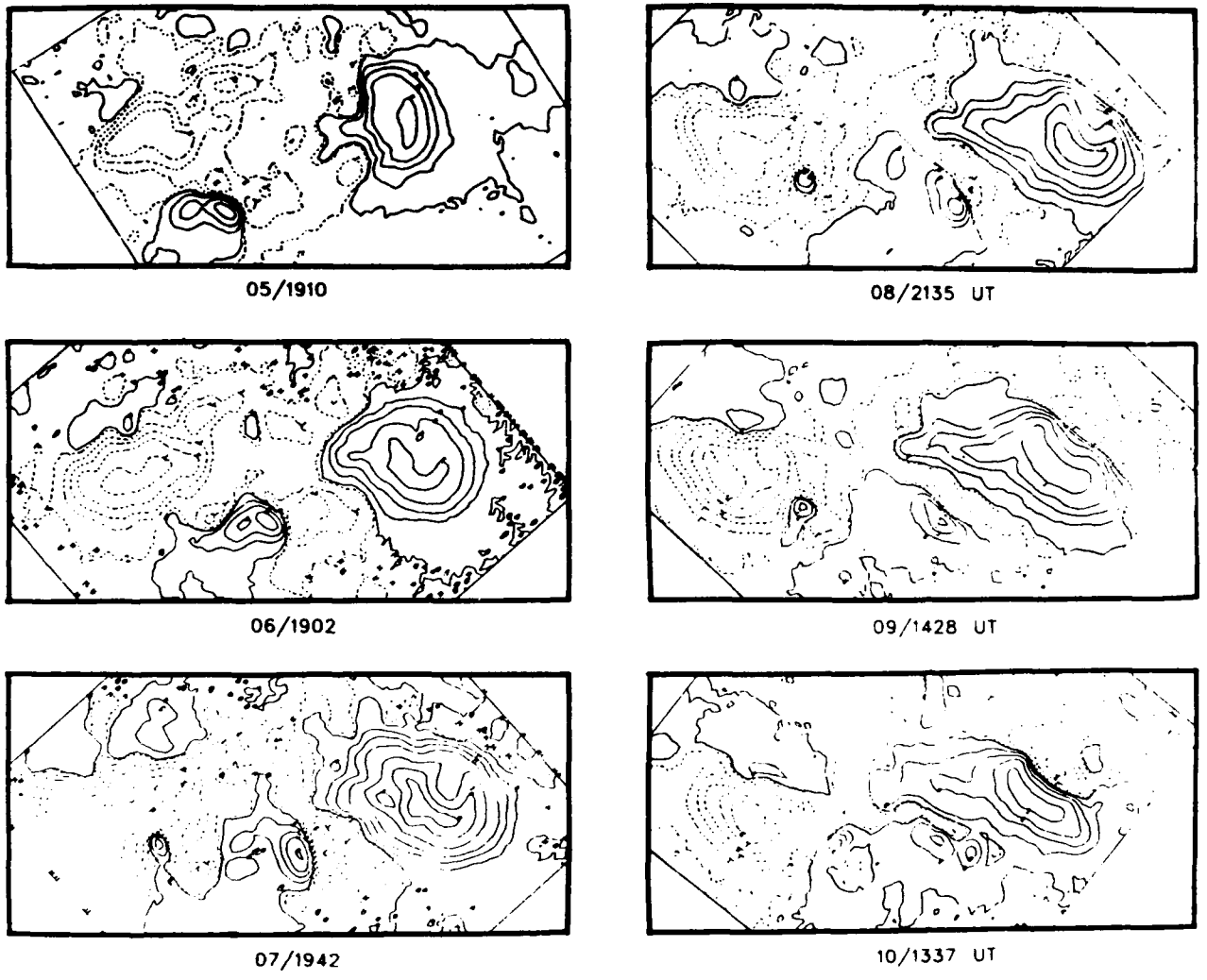

FIGURE II.1. The AR2372 longitudinal magnetic field (B_L) contours are depicted as solid lines (positive) and dotted lines (negative). Daily magnetograms for the period 5-10 April 1980 are shown.

rather large and strong, and the emerging flux region (EFR) added significantly to the complexity of the magnetic field. The region's production of moderate sized flares had already commenced on April 5th (X-ray flare histogram shown in Figure II.2). Significant relative motion of the spots was also observed. The positive spot of the newly emerged bipole was moving westward (toward the large leading spot), appearing to sweep up the negative fields ahead and becoming the positive spot of a new delta configuration spot (Figure II.1, 6 April and later). The small negative spot (Figure II.1, just north of the positive area on the 5th) was observed to move eastward in approximately the direction of the large (negative) trailing spot, resulting for a short time (see Figure II.1 on the 6th) in a second, somewhat weaker, delta configuration, revealing further complication of the magnetic field structure. This photospheric shearing motion of opposite polarity sunspots internal to the active region was most pronounced between the 5th and the 7th, with a relative velocity of near 200 meter/second. By the 5th, and even more on the 6th, the transverse field directions (Figure II.3, note alignment on the 6th of transverse field with neutral line in area of delta configuration) indicated the presence of strong shear along the neutral line, with relatively strong magnetic fields. Flares, some major, were frequent (Krall et al., 1982; Wu et al., 1984). Hagyard et al. (1984) have quantitatively evaluated the shear along the neutral lines of the region and related it to the locations of the origin (X-rays and H- alpha) and chromospheric (H-alpha) kernels of the major flare

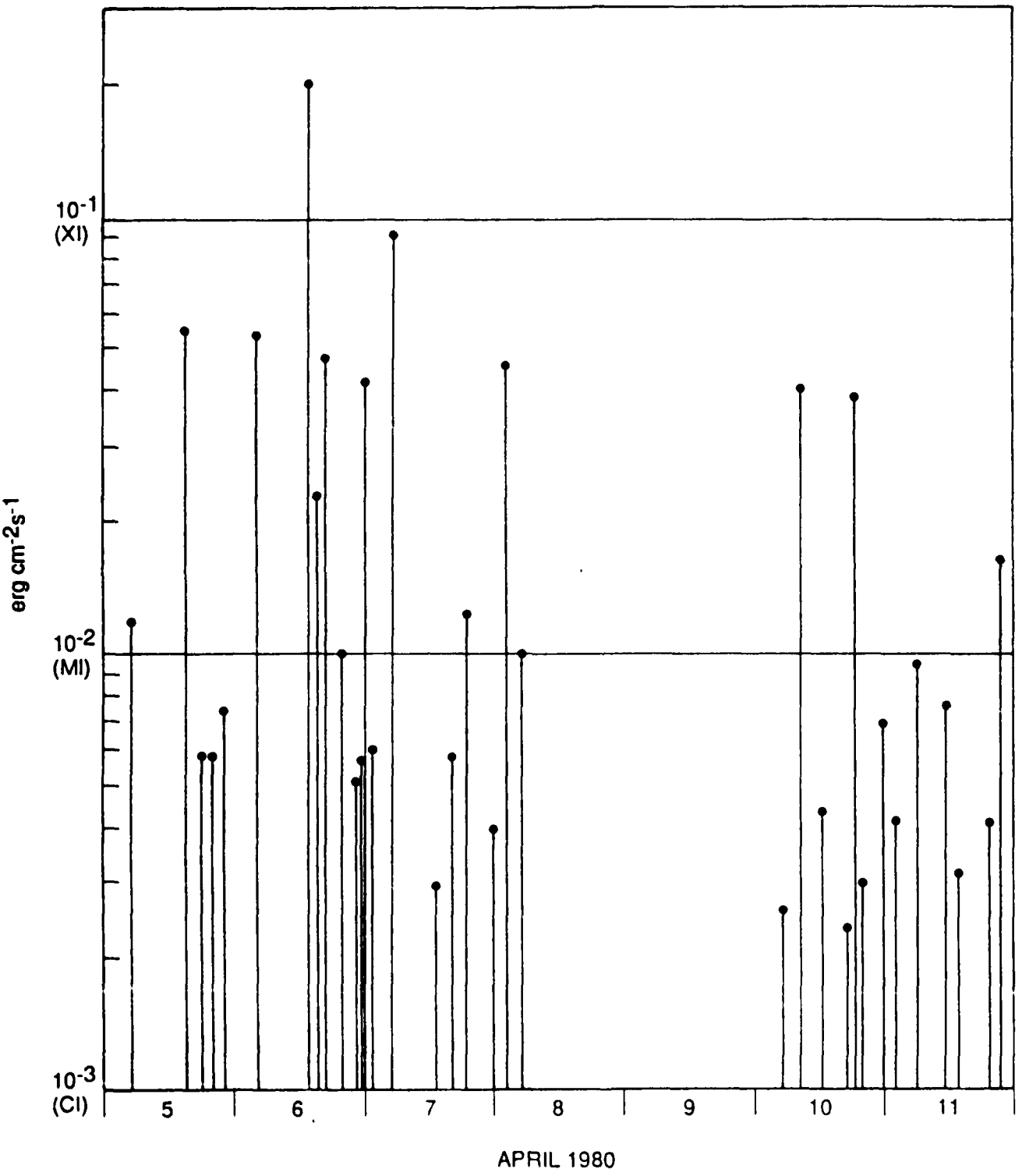

FIGURE II.2. AR2372 flare histogram. The x-ray flare classification (magnitude) is plotted for the signifcant flares.

EVOLUTION OF SHEAR IN TRANSVERSE MAGNETIC FIELD OF AR2372, APRIL 5-7, 1980

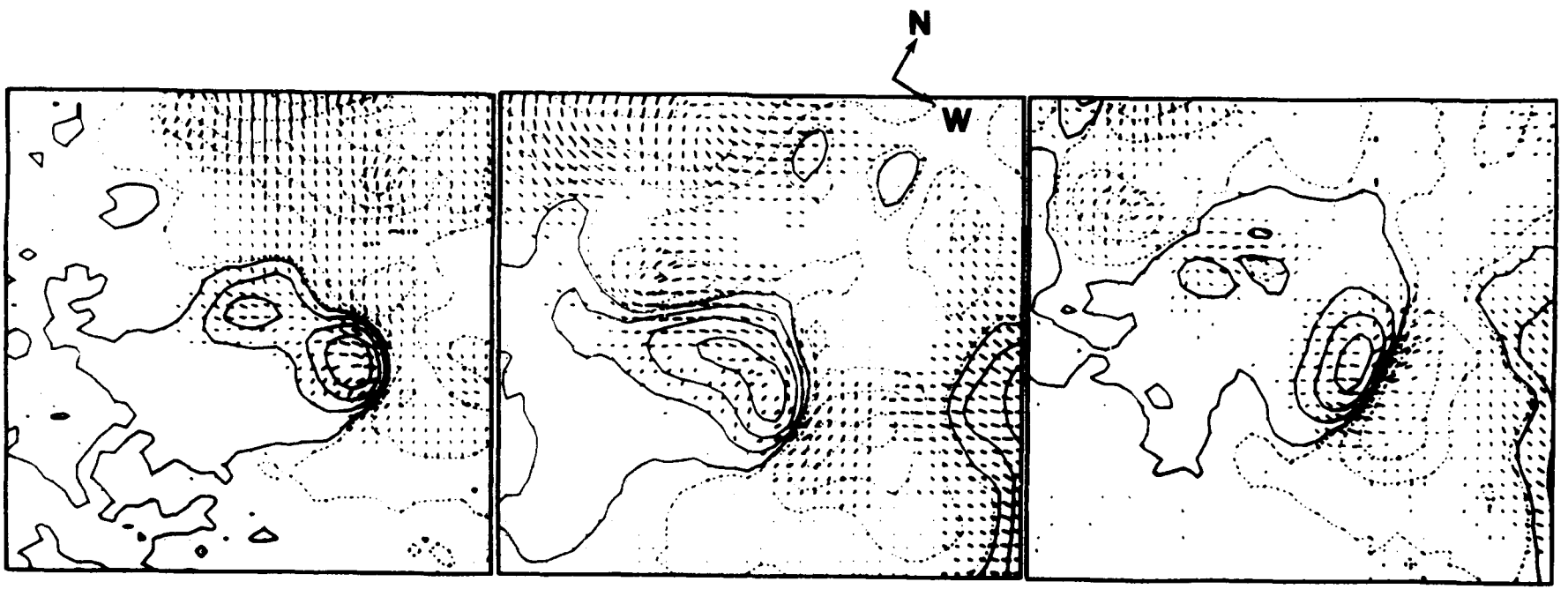

a. APRIL 5, 1980
1407 UT

b. APRIL 6, 1980
2055 UT

c. APRIL 7, 1980
1910 UT

FIGURE II.3. Evolution of the transverse component of the magnetic field in the dynamic southern bipolar portion of AR2372. Contours of B_L are superposed by line segments (A_z) representing the direction and relative magnitude (length of vector) of the transverse component of the vector magnetic field.

of the 6th. In fact, early analysis of the two regions, revealing that the AR2370 photospheric vector magnetic field was near potential in appearance and that AR2372 was increasingly sheared, strongly suggested that significant activity was most likely to occur in AR2372. A decrease in AR2372 shear after the 7th was followed by a temporary lull (see Figure II.2) in flare production.

AR2776: Another excellent example of the evolution/development of shear within an active region is shown in Figure II.4. Selected dates during rapid evolution are shown in Figure II.5 (longitudinal magnetic field contours) and Figure II.6 (longitudinal overlaid with azimuth vectors). AR2776 (November 1980), was another well observed SMM interval active region. From first observation AR2776 was an interesting region, containing a delta configuration and with some magnetic complexity. In Figure II.4a, on November 2nd, the intruding negative polarity spot of the delta configuration, to the southeast of the large positive polarity spot, introduces complexity. The magnetic field is moderately strong, and gradients are moderate. The same things can generally be said about the 3rd and the 4th (Figure II.4b and II.4c, and enlarged in Figure II.5a), except that some growth in the positive fields to the north, and some increase in the negative field strength of the intruding spot, result in stronger fields along the neutral line and an increase in gradient. Inspection of the Azimuth plot for the 2nd (Figure II.4a the vector-like line segments overlaid on the longitudinal field contours) reveals a generally (but not

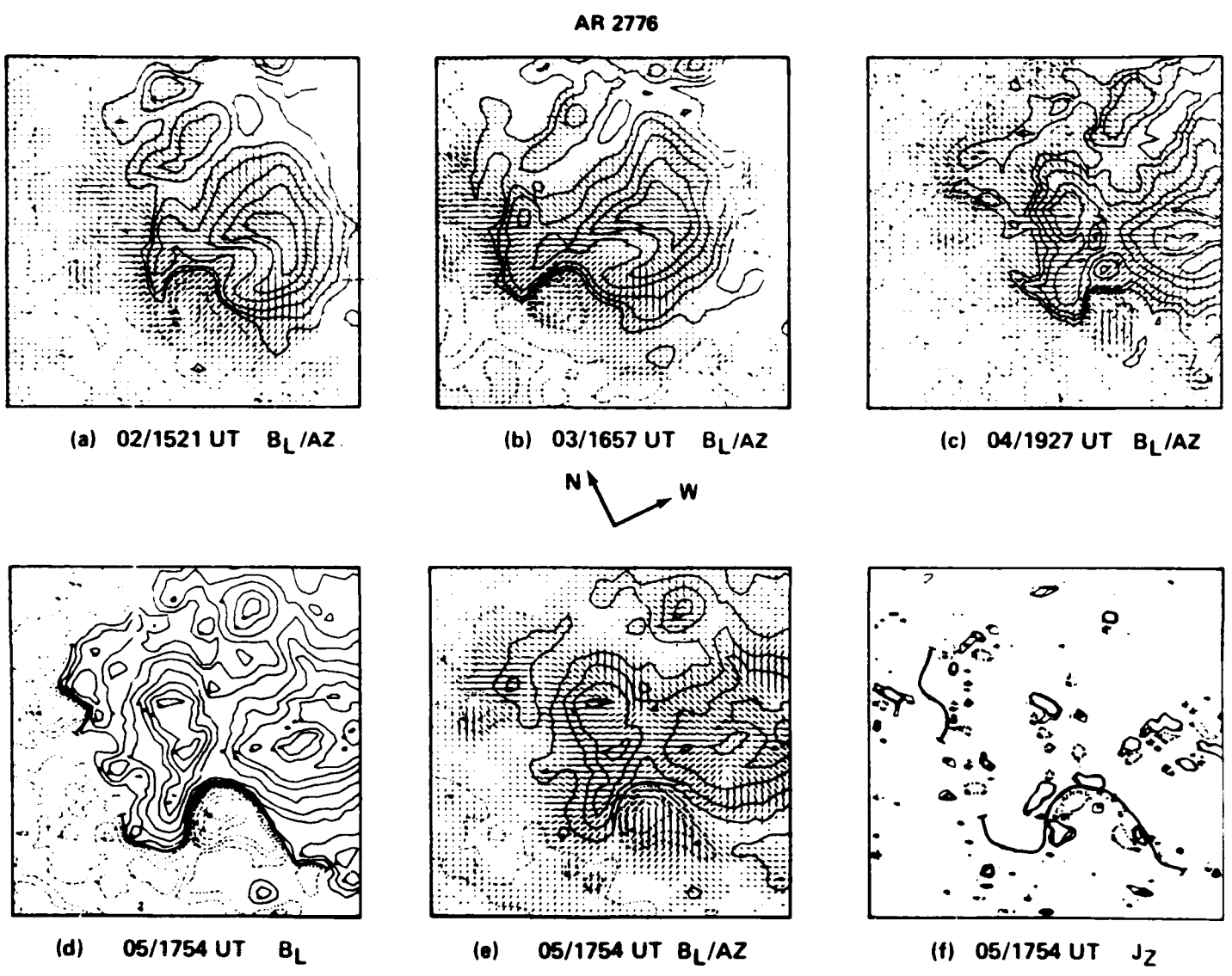

FIGURE II.4 AR2776 vector magnetic field evolution. In (a), (b), (c), and (e), the B_L contours are superposed by Az (transverse field) line segments, depicting strength and direction of the transverse component of the vector magnetic field. In panel (d), low order B_L contours are emphasized, to better illustrate the $B_L = 0$ (neutral) line. Panel (f) depicts the vertical current (J_z), as calculated from the transverse magnetic field. Nuetral line segments are duplicated in (d) and (f).

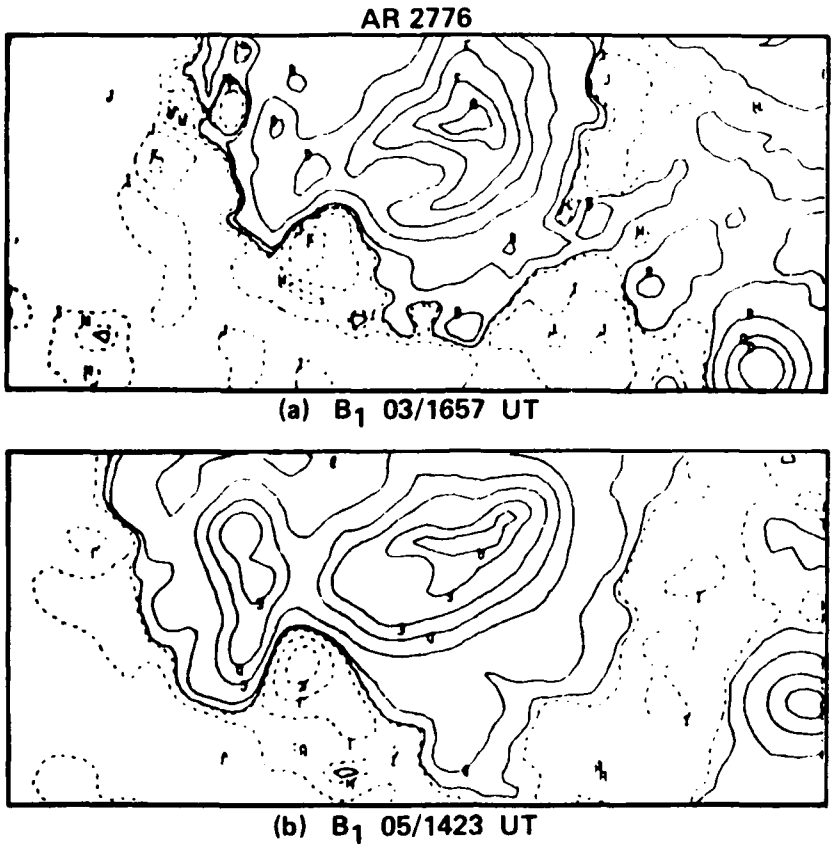

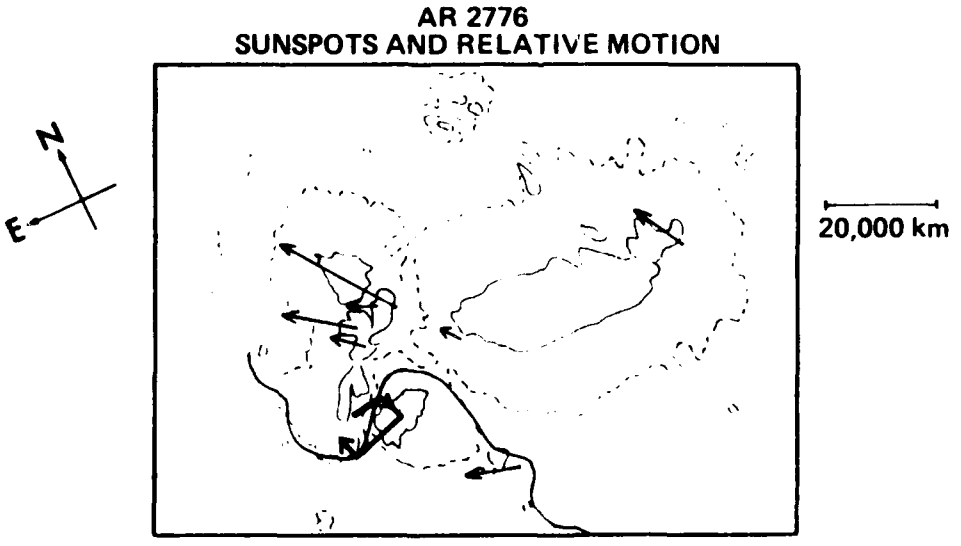

FIGURE II.5. AR2776 B_L and sunspots for the area of interest. Contours of B_L for the 4rd and 5th are shown in (a) and (b), illustrating the evolution of the longitudinal field during the interval of shear buildup. Solid lines represent positive field and dashed lines represent negative field. Sunspots are outlined in the solid lines (umbrae) and dashed lines (penumbrae) in (c).

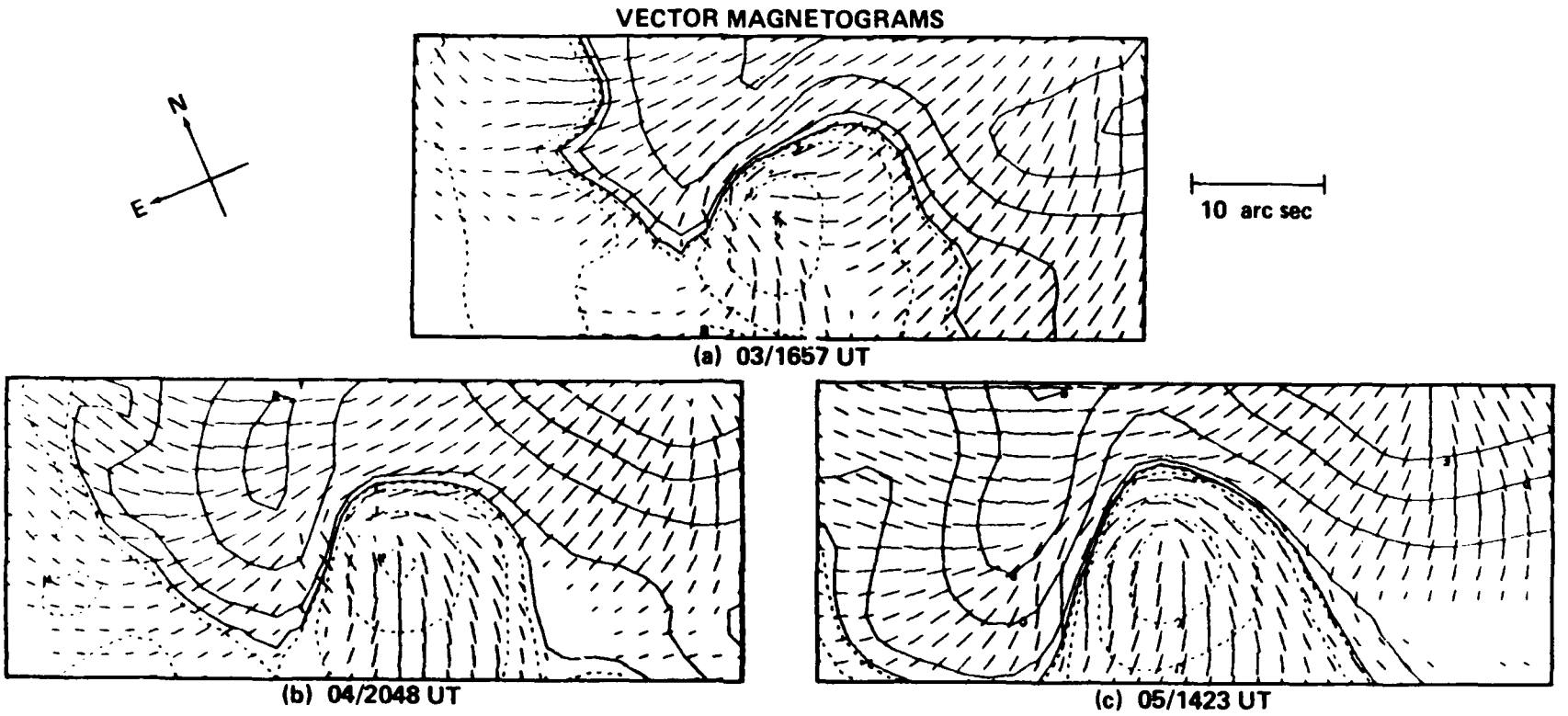

FIGURE II.6. The buildup of shear along the neutral line bordering the intruding negative polarity is shown for the interval 3-5 November 1980. The longitudinal magnetic field maps for the area of interest in AR 2776 are enlarged and superposed with Az vectors (to illustrate the direction and magnitude of the transverse component).

completely) potential appearing transverse field, aligned more or less directly from the large positive center to the negative portion of the delta. This is essentially true also on the 3rd (Figure II.6(a)), but with some complexity added by the building of the positive fields to the north. Continued complexity is added on the 4th, but, although complex and strong, the observed shear is not extensive. The changes between the 4th and 5th (Figure II.6b and II.6c) are striking, particularly in the pronounced shear - the near alignment of the strong transverse field (as seen in the azimuths) with the entire length of the longitudinal neutral line separating the intruding negative of the delta from the positive area(s) to the north. It must also be remarked that field strengths and gradients have continued to increase as the breakaway positive fields to the north and east have continued to build. This can easily be seen in Figure II.6b and II.6c, where contours are of the same values as for earlier plots. As shown in Figure II.7 (a histogram of X-ray flares for AR2776), early energetic soft x-ray flares (class M1 or greater) were infrequent. In fact, even lesser flares were infrequent prior to the 4th and, until the 5th, were located in the northern portion of the region. From the 5th, frequency and magnitude of flares rapidly increased, and the location of flare production shifted to the sheared delta configuration in the south. As discussed elsewhere in the report, the orientation of the transverse component is also implied by the orientation of the fibrils in the (H-alpha) chromosphere. In this case, the observed field azimuth (from photospheric vector magnetograms) on

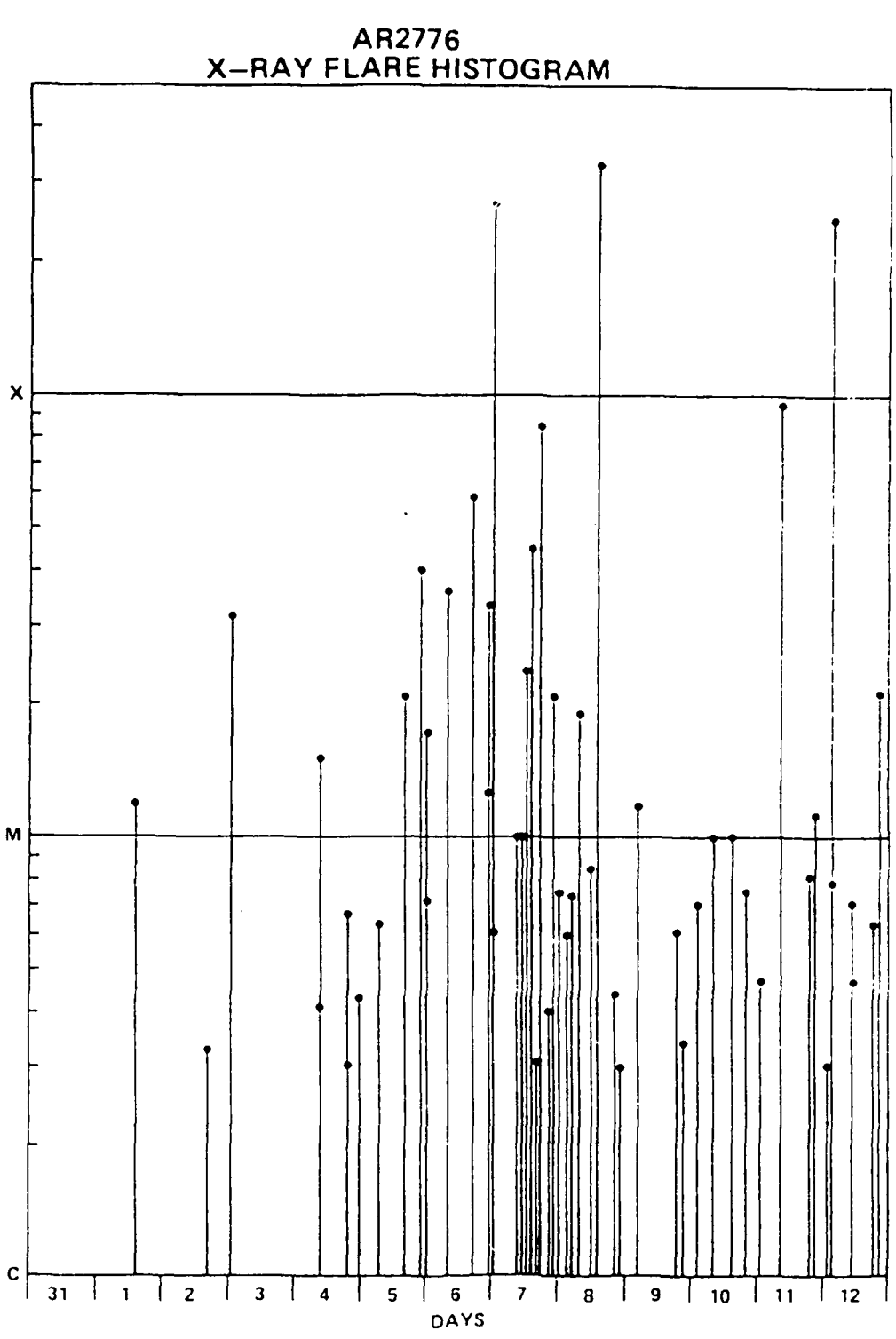

FIGURE II.7 X-ray flare histogram for AR2776. X-ray flare classification (magnitude) is plotted for the interval of disk transit.

the 5th (Figure II.6c) compares well with the fibril structure seen in Figure II.8 (SOON H-alpha filtergram) further substantiating the existence of strong shear along the neutral line of the delta configuration. As an example of the family of flares originating in this highly sheared area, the large (X-ray class M4) flare of the 5th is shown in Figure II.8 (SOON H-alpha on band) and Figure II.9 (SOON H- alpha off-band and HXIS hard x-rays). The points of initial brightening in the November 5 flare, as well as the kernels of greatest chromospheric intensity, were located in the area of maximum shear. These kernels can be seen in in the H-alpha off-band filtergram of Figure II.9, where, in addition, SMM/HXIS observed hard x-ray emission contours are also shown. Neidig et al. (1986) discussed the evolution of the magnetic field, the motion of the sunspots within the region, and the relationship of shear to the region's early flare production. J_z the vertical component of current, as calculated from the transverse component of the magnetic field, is shown in Figure II.4f. In order to make clear the relationship of the J_z maxima to the neutral line, segments of the neutral line are superposed and can be compared to the same segments as shown in the longitudinal magnetogram (Figure II.4d.)

AR4711, a highly productive active region, is of particular interest, partially because of its development late in the declining phase of the solar cycle. It rotated onto the visible disk near the end of January, 1986, and, in initial configuration it appeared to be a primarily unipolar spot, typical of a region late in its evolution. Beginning with February 3, when vector

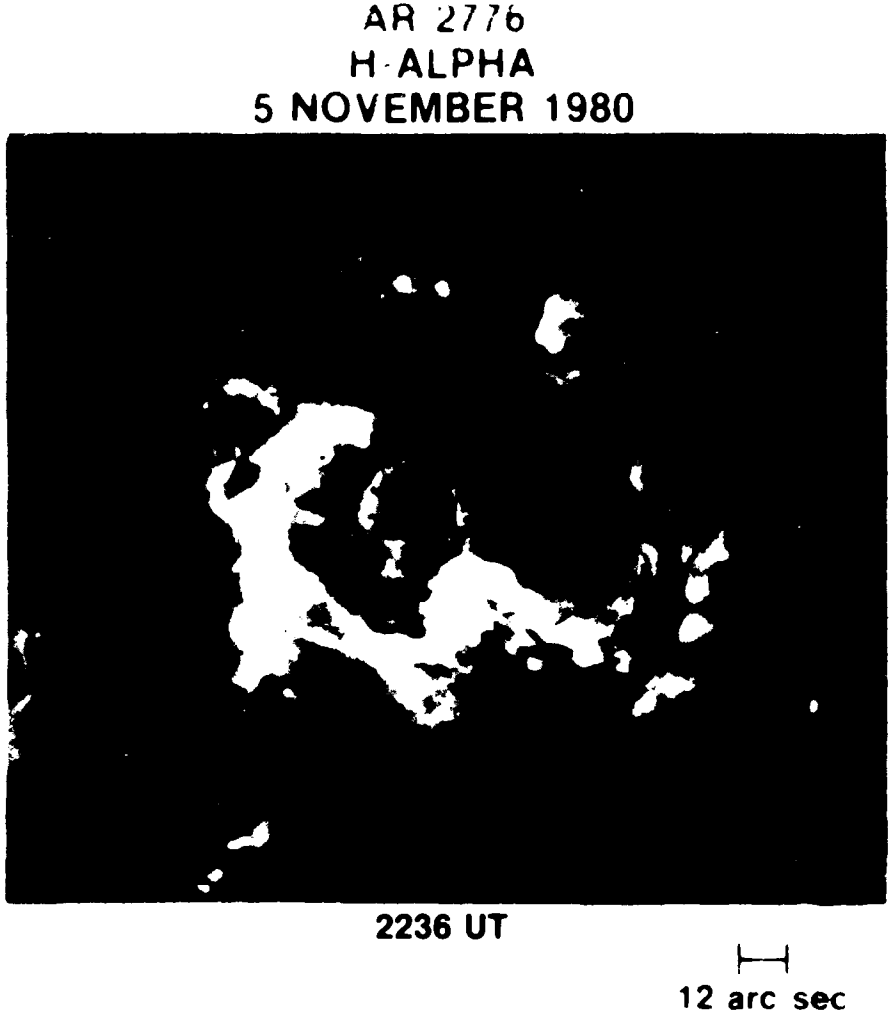

FIGURE II.8. Hydrogen Alpha filtergram of AR2776 during a large flare on 5 November 1980. Note the alignment of absorption featues with the neutral line, indicating a strongly sheared magnetic field (High resolution H-alpha filtergram courtesy AWS/SOON observatory).

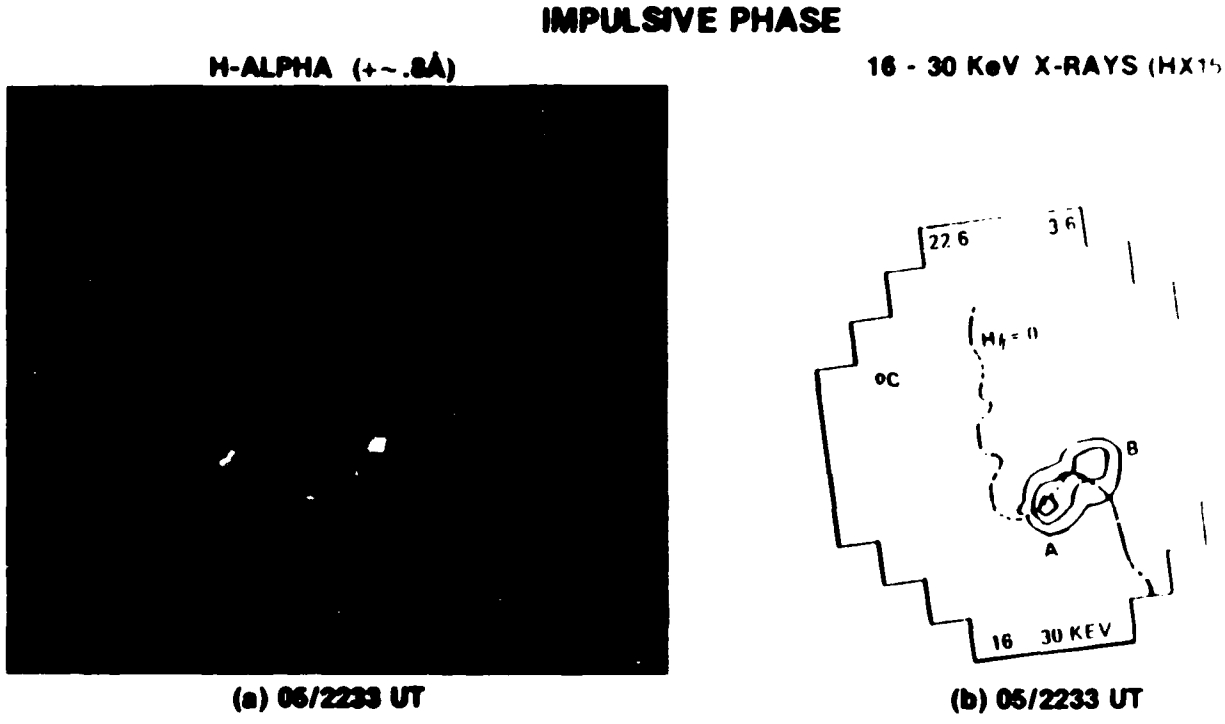

FIGURE II.9. Off-band H-alpha filtergram (a) during the large flare of 5 November 1980, showing the intense kernels of the flare (as seen at line center in Figure II.8). The location and offset of the footpoints of the intense flare elements illustrates the sheared nature of the magnetic field, and can be compared with the hard x-ray loops (and footpoints) observed by HXIS and shown in (b).

magnetograms begin, the long term evolution of AR4711 is shown in Figures II.10, II.11, and II.12. In Figure II.10, contours are of circular polarization, representing the line-of-sight (or longitudinal) component of the magnetic field (B_L). In Figure II.11, minimum (5 gauss) B_L are superposed on Az (transverse) vectors , and in Figure II.12, intensity contours depict sunspots. The long term (westward) clockwise proper motion (relative to the large positive sunspot) of the negative polarity center of area A (from Figure II.13), and the associated area of strong shear, can be clearly seen in Figures II.10, II.11, and II.12. By 03\1642 UT (Figure II.13a), the region had developed considerable complexity, with four areas (labeled A, B, C, and D in Figure II.13a and II.13c) with apparent flare originating capability. Based on the analysis of parameters discussed above, area A, with strong shear, strong fields, a large gradient, and relative (shearing) sunspot motion, was considered the most likely location for significant flare production, followed by area B, where shear was also present. (The area A available energy buildup can also be demonstrated by MHD simulation.) Areas C and D, although believed possible flare sources, were less promising - primarily because significant shear was not observed (see Figure II.13). In fact, large flares were primarily originated at area 'A', with flare kernels located either side of the area 'A' neutral line. During the "flash" phase, the large flares then rapidly spread along the neutral line in area "B". A flare frequency and magnitude histogram for AR4711 is shown in Figure II.14. With vector magnetogram

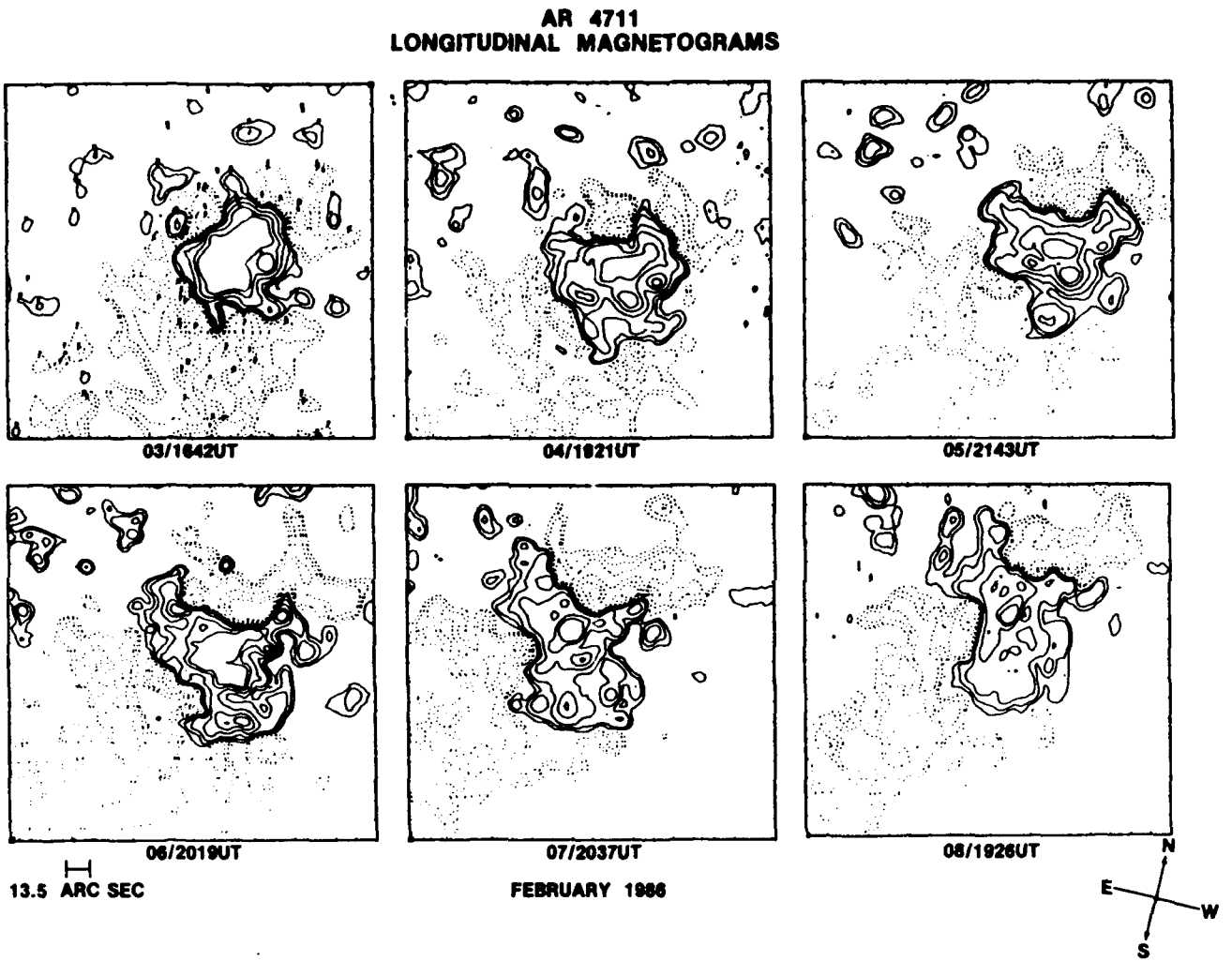

FIGURE II.10. AR4711 B_L evolution for the period 3-8 February 1986. Solid contours represent positive and dotted lines negative magnetic field. Note the proper motion of the northern negative center.

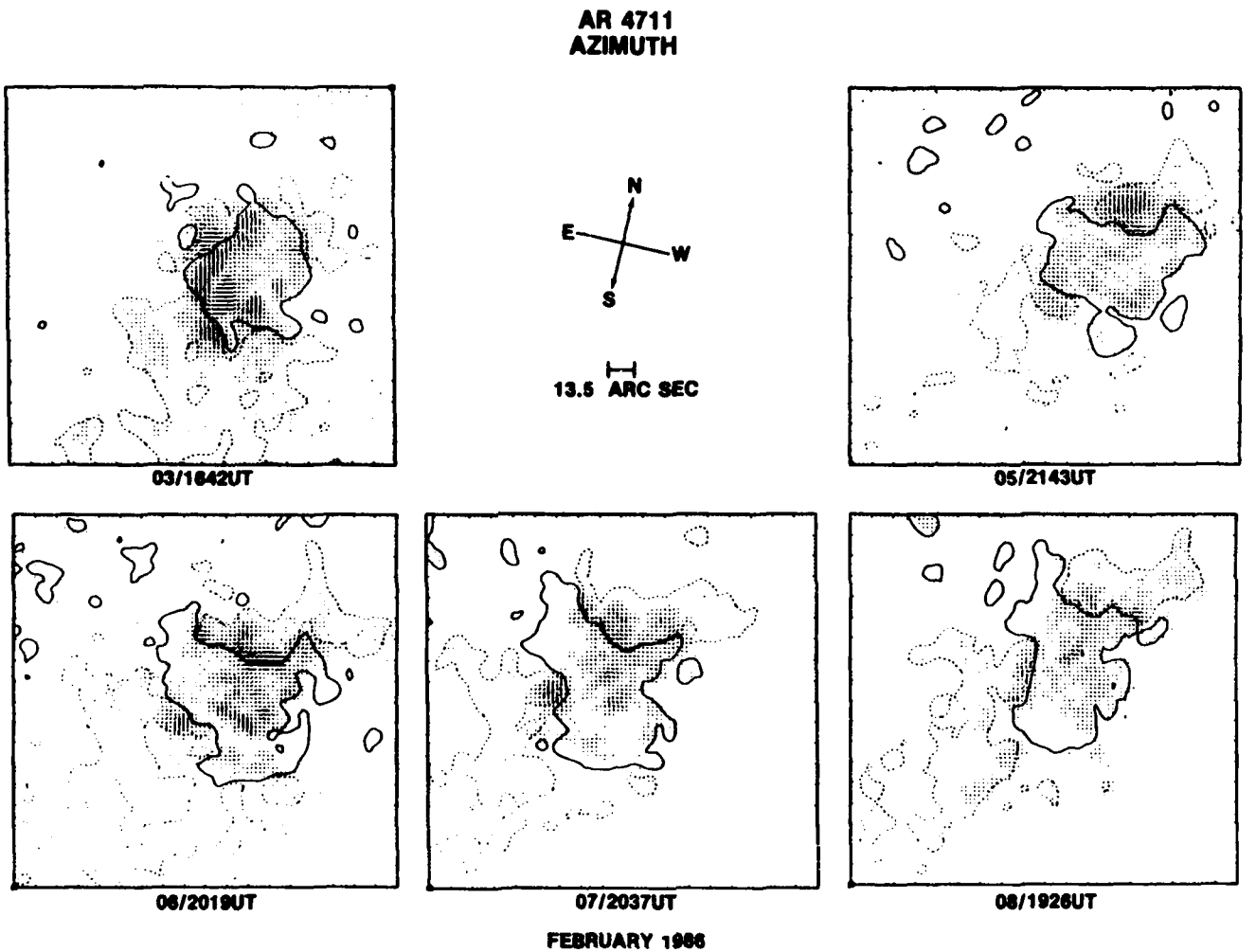

FIGURE II.11. Az (transverse component) evolution for the period 3-8 February 1986 (the 4th is missing) superposed minimum contours (±5 gauss). The minimum contours are used to illustrate the approximate location of the (B_L) neutral lines.

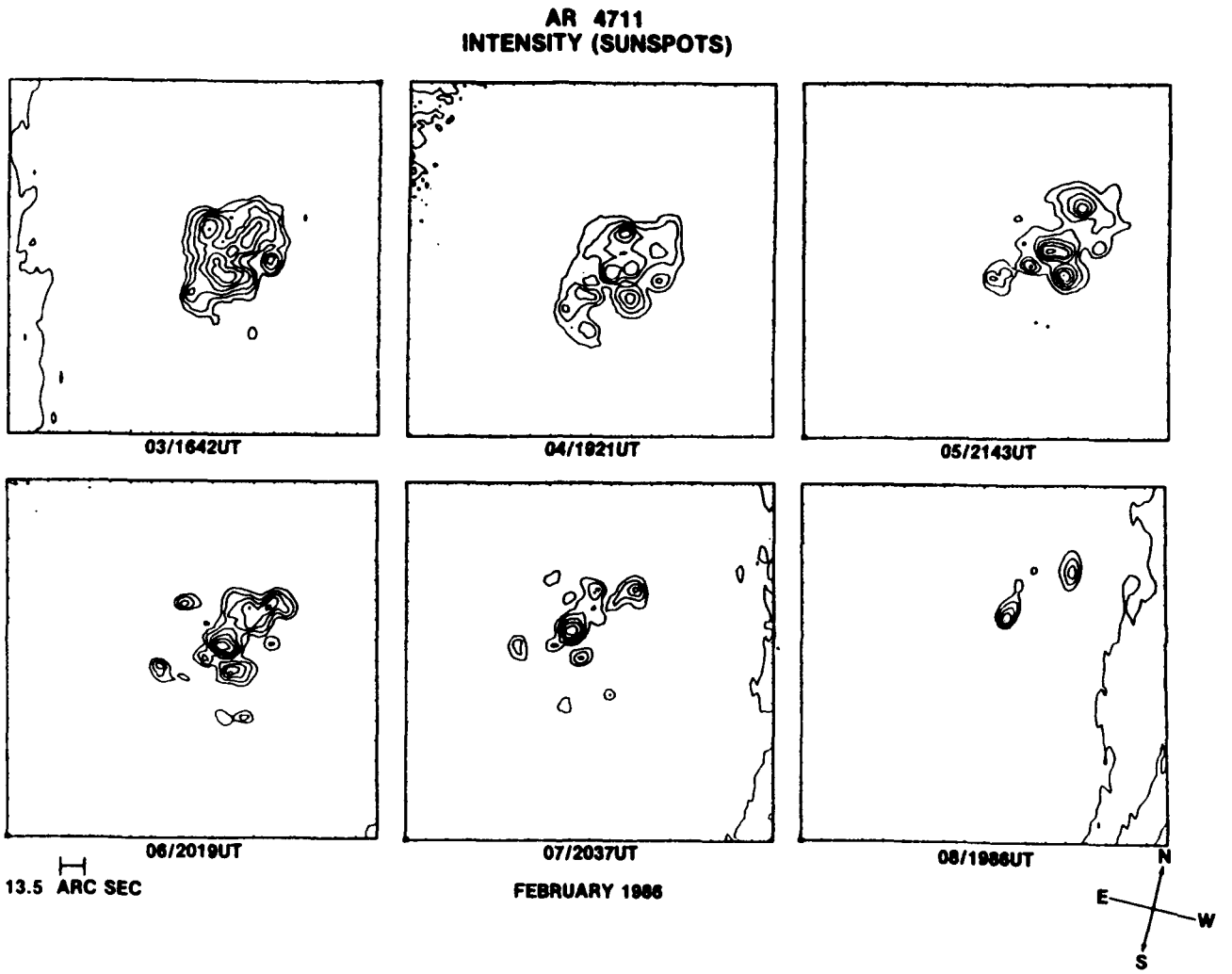

FIGURE II.12. AR4711 intensity contours depict approximate sunspot outlines for each day during the interval 3-8 February 1986.

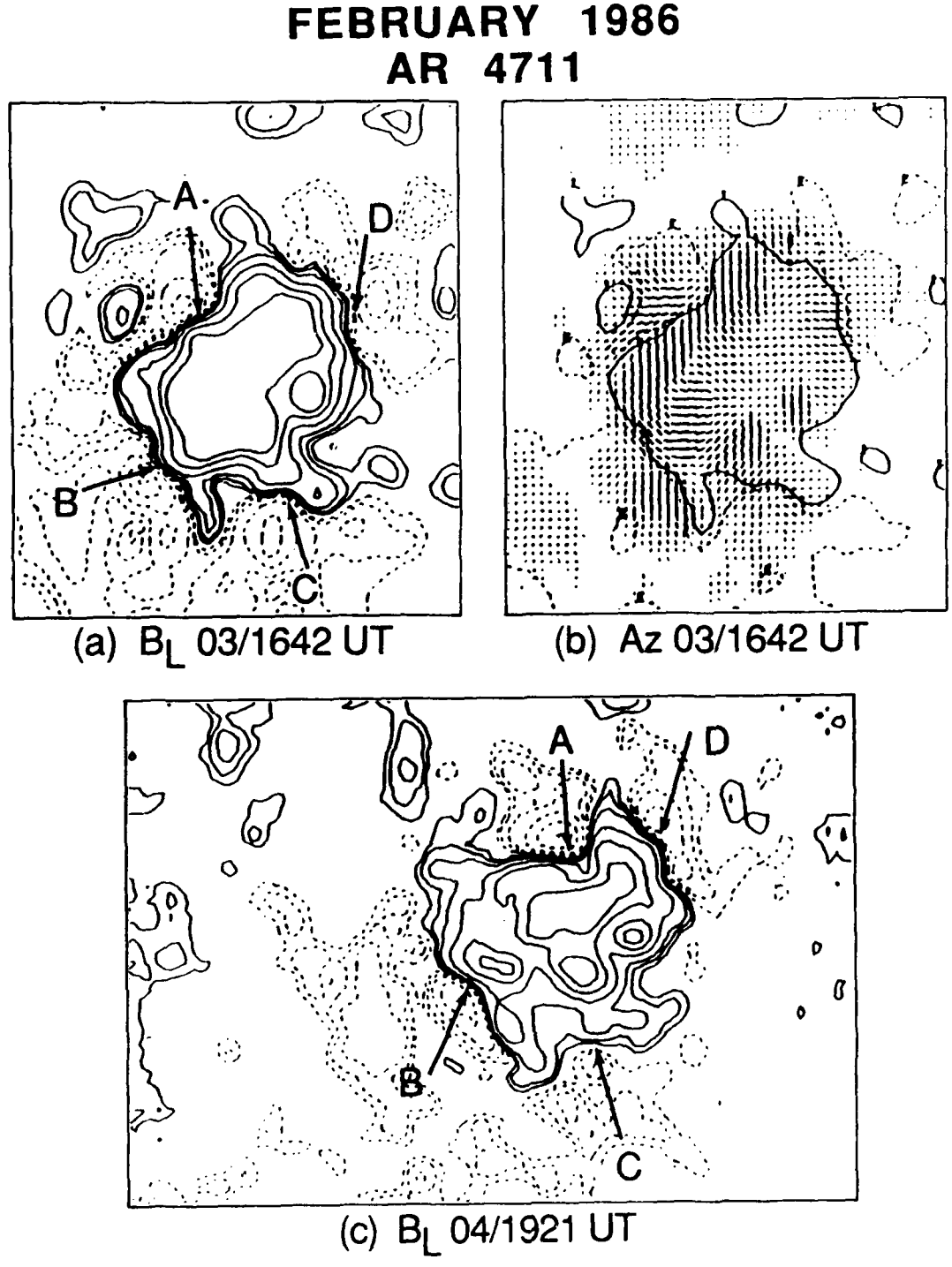

FIGURE II.13. AR4711 Enlarged longitudinal magnetograms are shown for 3 (a) and 4 (c) February 1986. Possible flare sites are indicated (in descending order of flare potential) as A, B, C, and D. Again, note the proper motion of A. In (b), low order positive and negative contours indicate approximate positions of neutral lines and are overlaid by Az line segments. Note the strong shear at locations A and B. Sites and activity are discussed in the text.

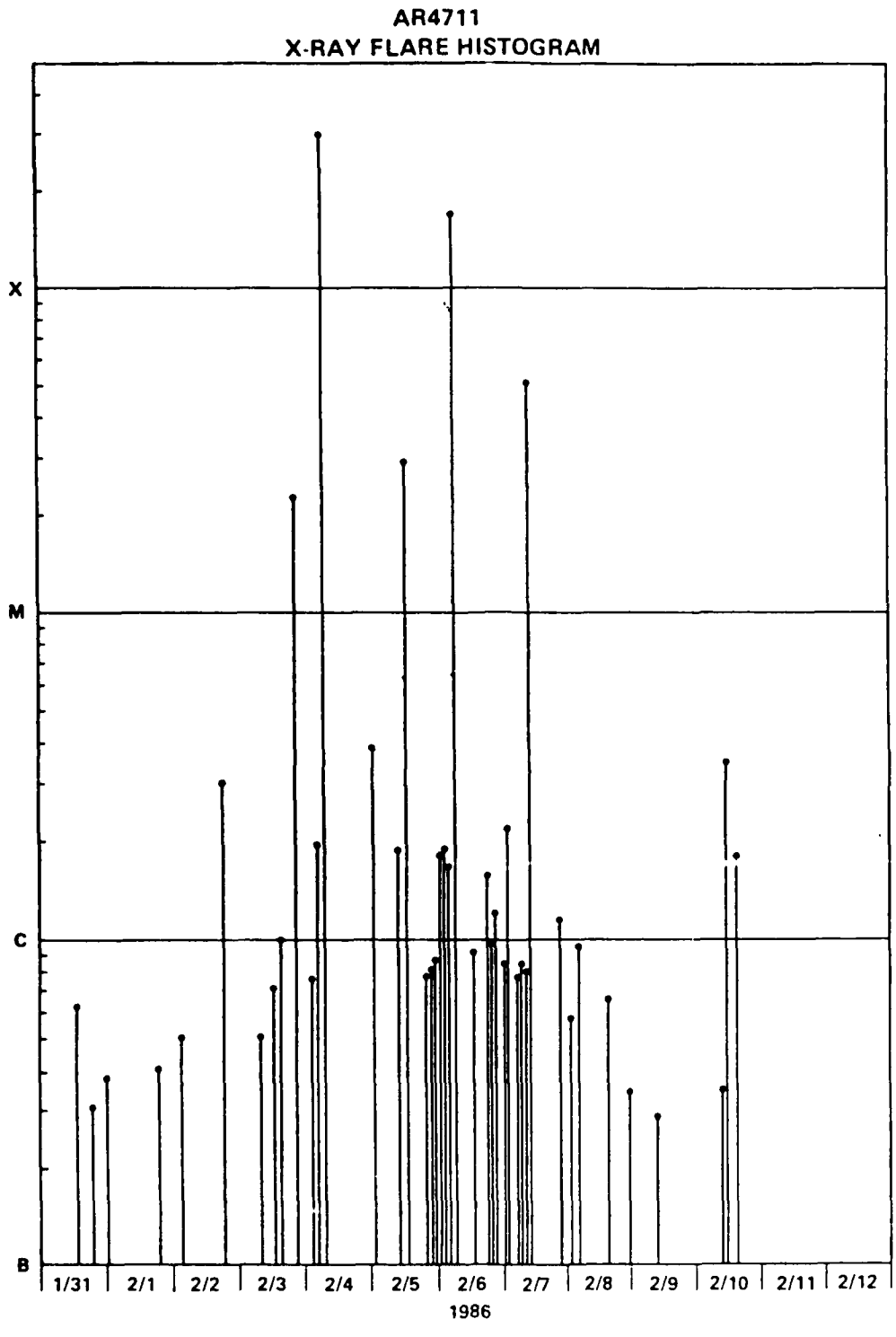

FIGURE II.14. X-ray flare histogram for the disk transit of AR4711.

calibration and the calculated potential field, AR4711 shear index parameters (as defined early in Section II.3 and in Table II.2) will be quantitatively analyzed AR4711. With the pronounced long-duration proper motion of area 'A', AR4711, is also a near-term candidate for MHD analysis.

In Figure II.15, where B_L (longitudinal contours), A_z (azimuths transverse component), and the J_z are shown for three less complex and less productive (but nevertheless interesting) regions, longitudinal neutral line segments of interest are overlaid for comparison with the direction and relative magnitude of the transverse field. AR2725 (panels c and d), the most complex and interesting of the three regions, was also the most flare productive. Examination of the azimuth plot reveals significant shear (near alignment of azimuths with neutral line), along with moderate field strengths, along the simple north-south portion of the northeastern neutral line, separating moderately strong positive and negative closed contours (probably spot umbrae). Additional weak shear is seen along the simple neutral line in the northeast field of view. Although significant flares were infrequent, a few class M x-ray flares and a major flare (an X3/3B, 3 days after these magnetograms) were observed. (A smaller flare, a C7/1B, was observed about midway between the two magnetograms.) AR2522 (panel a) has complexity in the form of a convoluted neutral line and an isolated area of positive polarity. Examination of the azimuths, with overlaid neutral line, reveals only weak shear along the southern (east-west) boundary of the large intruding peninsula of positive polarity.

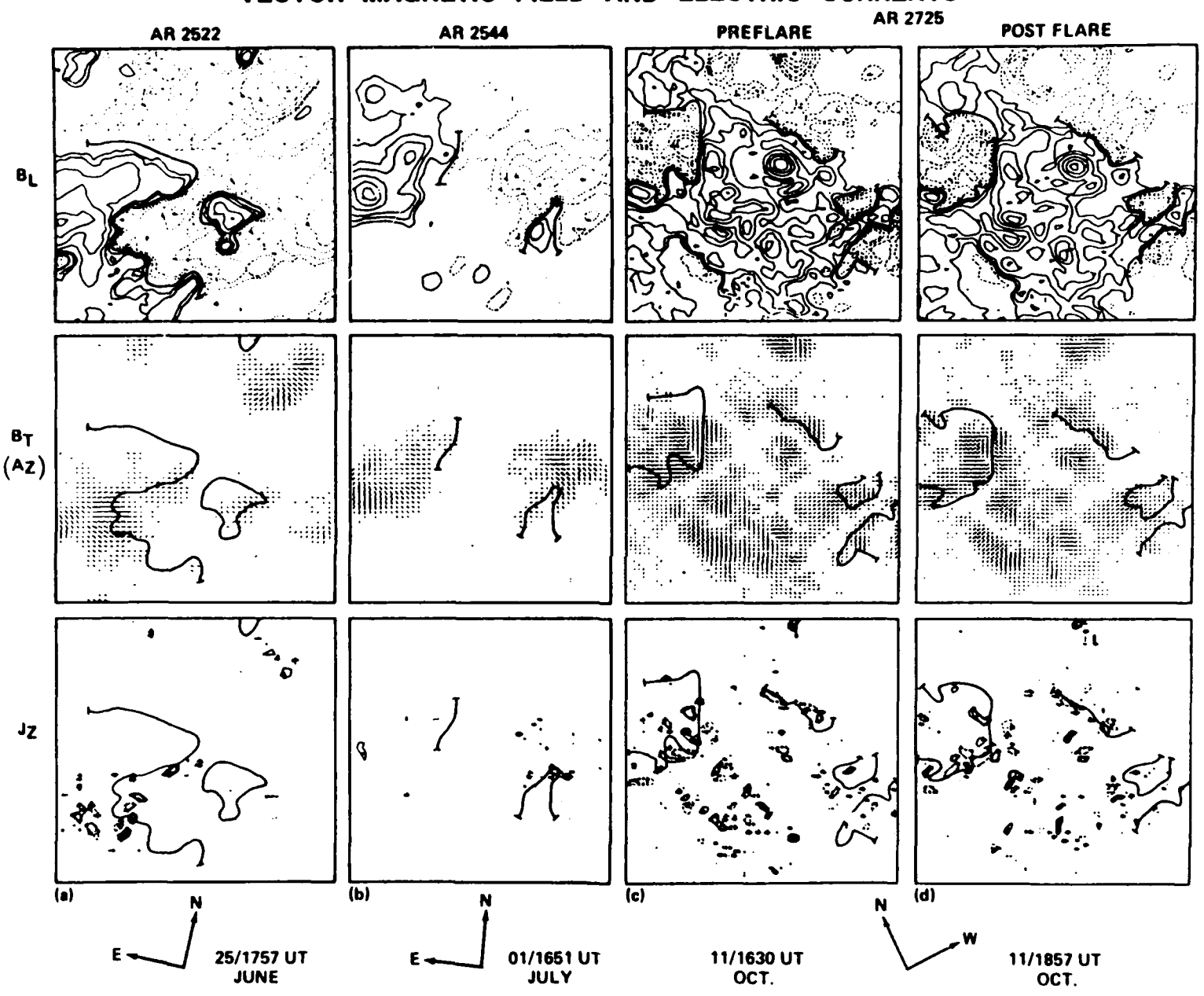

FIGURE II.15 Longitudinal magnetograms, Az vectors, and calculated Jz the shown for three regions during 1980. To facilitate mental registration and comparison of features, B_L neutral lines are drawn on each panel. Two sets of data are shown for AR2725.

The region produced numerous minor flares, with a few small class M (M1 to M4) events during its disk transit. AR2544, with only the minor complexity of the isolated positive spot intruding from the south, into the negative, leading portion of the region, is something of a counter example. There is clearly no evidence of strong or extensive shear, nor is the transverse magnetic field strong along the neutral line. There is only the magnetic field complexity implied by the intrusion of opposite polarity. The region, born near central meridian on about the 28th of June, produced only a few flares. However, this included a rash of activity on June 30th, including an M1 and, spectacularly, a major flare (class X2) on July 1st, the day of the illustrated magnetogram - followed, essentially, by no significant activity.

3.2 Activity Correlation - General Discussion

The initial analysis (in some cases, preliminary) of several active regions, including those discussed above, is summarized in Table II.1. The occurrence of flares is compared with the observational parameters considered most promising in flare prediction; these are the initial parameters to be included in the test flare index. (The MHD analysis and projection parameters are not included, nor is sunspot motion, due to inadequate representation within this data sample. Those parameters will, however, be a part of the test composite flare predictor in cases where available.) It is not surprising to find that the AR2372, AR2776, and AR4711 (all discussed in Section 3.1 above), were characterized by features which we associate with significant flare production, and that the sheared

areas within those regions were indeed the site of the onset of frequent and significant flares. There is also good correlation between the presence of more-or-less potential magnetic fields and the lack of significant flare production. There are, however, some cases that are less clear. In particular, AR2544, discussed above and pictured in Figure 15, had a short period of surprising high flare production. Cases of this sort can only be adequately analyzed with high temporal resolution vector magnetograms and high spatial and temporal resolution H-alpha (SOON filtergrams), neither of which is available for this period.

3.3 Declining Cycle and Expectations

Independent testing and refinement of forecasting techniques based on the parameters discussed in this report, and using a tentatively defined "shear index", depends on increased activity - probably associated with the new solar cycle. The development and activity level of the new cycle (cycle 22) can not yet be predicted with confidence, but recent solar behavior implies a significant new cycle onset. AR4711 and AR4713, both of which transited the disk in February of 1986, were of the old cycle (low latitude), and produced a typical, temporally isolated spurt of activity. However, there have since been several high latitude regions clearly of the polarity configuration of the new cycle. One of these regions was moderately large, with a moderate level of activity (including a Class M flare). Further development, testing, and application is dependent upon an adequate observational program, in both magnetograms and high-

resolution Hydrogen Alpha. Again we strongly encourage and request AWS/SOON cooperation/collaboration in acquiring high resolution H-alpha and sunspot observations during the transit of appropriate active regions.

III. Modelling

1. Theory

It has been demonstrated through magnetohydrodynamic (MHD) theory that photospheric motions control the evolutionary dynamics and the structure of fields and currents in an active region (Wu et al. 1983; 1984, 1986, 1987). These results have shown that the occurrence of flares is strongly correlated with the locations of concentration of fields and currents, as well as with the dynamical motion of the plasma. From the recent observational studies, it has been shown by Hagyard et al. (1984) and by the data presented in Section II, that the observed shear in photospheric magnetic fields could be related to significant and repeated flaring. DeLoach et al. (1984) found that the photospheric electric currents, deduced from the observed sheared photospheric magnetic fields (data acquired by Marshall Space Flight Center's vector magnetograph), were correlated with the transition region brightness, as observed by ultraviolet spectroheliograms on board the Solar Maximum Mission Satellite. Recently, it has also been shown by Smith, Jr. et al. (1983) that in analyzing active regions, observed shear is well-correlated with the occurrence of flares, and that a quantitative representation of shear (a shear index) can be used in the determination of an active region's potential for major flare

production, which may lead to improvement in flare prediction techniques, in which this shear index could also be deduced from model calculation and will be compared with the observation].

From the theoretical point of view, it is believed that most of the energy released in flares is stored in the magnetic field (Van Hoven, 1980) in the form of electric current (Calquist, 1972), and that the energy release may be triggered by a magnetohydrodynamics (MHD) instability, such as the commonly discussed resistive magnetic tearing mode (Van Hoven, 1979). This energy-storage and energy-release cycle can be a mechanism for field reconnection, which may lead to observable consequences such as the solar flares. The important physical parameters used to determine the MHD instability criteria are the local magnetic field strength and the gradient of magnetic field, as well as the plasma flow velocity. These parameters are directly related to the occurrence of the flare, as suggested by Smith, Jr. (1984). Therefore, we shall use a self-consistent magnetohydrodynamic (MHD) model as given by Wu et al. (1983) to compute those parameters and to attempt to reveal the physical mechanisms for the flare occurrence, which may enhance the current techniques used in the flare prediction.

1.1. Basic Equations

The physical system under consideration is a general case of a transient magnetohydrodynamic (MHD) flow in which an initial steady state is subject to a finite amplitude disturbance. Because of the limitation of the memory capacity of the available computer, we shall use a two-dimensional, nonplanar, time-

dependent, ideal MHD equation, defined in rectangular coordinates, for this study. In the ideal MHD equations, all dissipation terms (i.e. thermal conduction and finite electric resistivity) are ignored. However, these effects will not influence the generality of the present suggested method. According to the description mentioned above, the governing equations for this MHD flow can be expressed in the following form:

$$\frac{\partial \rho}{\partial t} = - \frac{\partial (\rho u)}{\partial x} - \frac{\partial (\rho v)}{\partial y}, \tag{1}$$

$$\frac{\partial (\rho u)}{\partial t} = - \frac{\partial p}{\partial x} - \frac{\partial}{\partial x} (\rho u^2) - \frac{\partial}{\partial y} (\rho uv) + B_y \left(\frac{\partial B_x}{\partial y} - \frac{\partial B_y}{\partial x} \right) - B_z \frac{\partial B_z}{\partial x}, \tag{2}$$

$$\frac{\partial (\rho v)}{\partial t} = - \frac{\partial p}{\partial y} - \frac{\partial}{\partial x} (\rho uv) - \frac{\partial}{\partial y} (\rho v^2) - B_x \left(\frac{\partial B_x}{\partial y} - \frac{\partial B_y}{\partial x} \right) - B_z \frac{\partial B_z}{\partial x} - \rho g \tag{3}$$

$$\frac{\partial (\rho w)}{\partial t} = - \frac{\partial}{\partial x} (puw) - \frac{\partial}{\partial y} (pvw) + B_x \frac{\partial B_z}{\partial x} + B_y \frac{\partial B_z}{\partial y} \tag{4}$$

$$\frac{\partial B_x}{\partial t} = \frac{\partial}{\partial y} (uB_y - vB_x), \tag{5}$$

$$\frac{\partial B_y}{\partial t} = \frac{\partial}{\partial x} (vB_x - uB_y), \tag{6}$$

$$\frac{\partial B_z}{\partial t} = \frac{\partial}{\partial x} (wB_x - uB_z) + \frac{\partial}{\partial y} (wB_y - vB_z), \tag{7}$$

$$\frac{\partial T}{\partial t} = - \frac{\partial (Tu)}{\partial x} - \frac{\partial (Tv)}{\partial y} + \frac{T}{3} \left(\frac{\partial u}{\partial x} + \frac{\partial v}{\partial y} \right), \tag{8}$$

and

$$p = \rho RT, \tag{9}$$

where u, v, and w are the three velocity components in x, y and z axis repectively, and B_x, B_y, and B_z the magnetic field components. The other notations are defined as: ρ is the density; T is the tempreature; g is the gravitation acceleration; p is the thermal pressure; and R is the universal gas constant. It is noted that we have suppressed the factor 4π in the term of Lorentz's force through an adequate choice of the unit of magnetic field.

1.2. Boundary and Initial Conditions

To initialize the computations, the boundary and initial conditions are needed. We shall summarize these conditions as follows:

1.2.1. Boundary Conditions

There are four boundaries to be specified for this investigation, as shown in Figure III.1: the bottom ($y = 0$) is a physical boundary; the top ($y = y_0$) is a computational boundary; and the two sides ($x = 0$ and $x = x_0$) are symmetric boundaries, since a periodic solution is chosen to represent the initial magnetic field. The mathematical details and accuracy of numerical code are published in a paper by Hu and Wu, (1984), the effects due to boundary conditions was studied by Wu and Wang (1987).

The initial conditions can be obtained by the steady-state solution of the set of governing equations (1) through (9). Physically, this is the undisturbed solar atmosphere. In the present study, we adopted an isothermal and hydrostatic equilibrium atmosphere (i.e. $T_0^0 = 10^5$ and $n_0^0 = 10^{12}$, where the

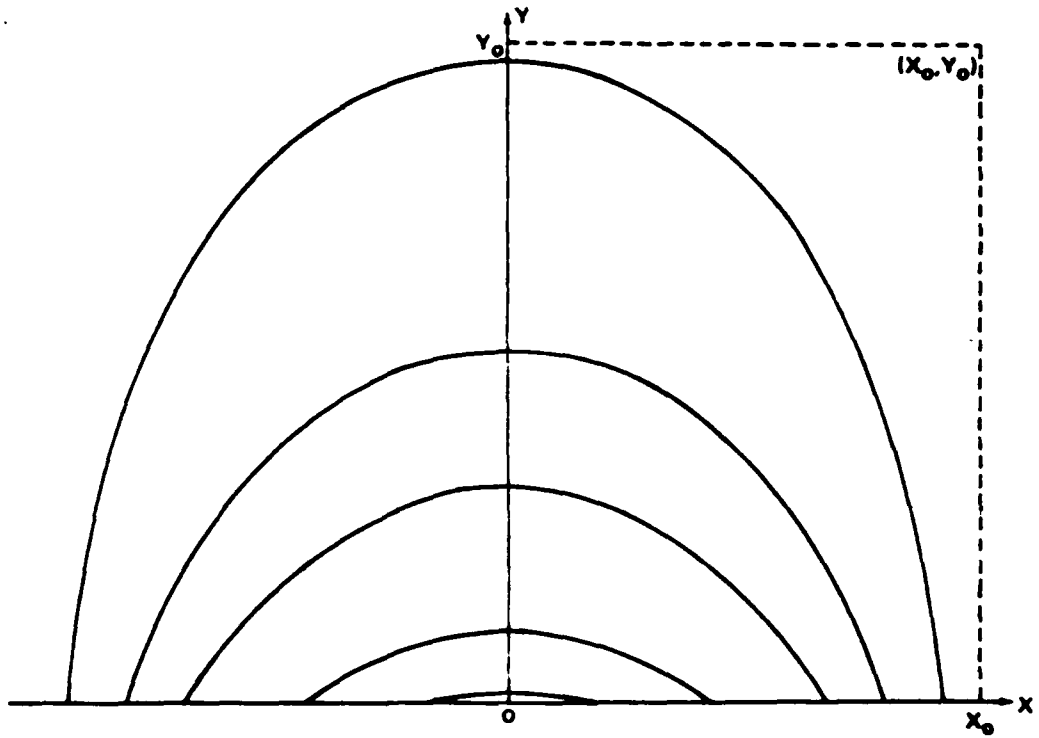

FIGURE III.1. The Initial Magnetic Configuration and the Computational Domain for a Representative Physical Problem that is Solved with the Present FICE Method.

subscript "o" indicates the location at the lower boundary and superscript "o" indicates the initial time). Following these initiation steps, a perturbation is introduced. In the present study, two different types of shear motion and two different values of β_0^0 (i.e. the ratio of plasma pressure to the magnetic pressure = $\frac{16\pi n^0 kT^0}{(B_0^0)^2}$) with a shearing speed of 1 km s^{-1} were used. A schematic representation of these perturbations is shown in Figure III.2 and the numerical results obtained from the model are discussed in the next section.

2. Numerical Results

In this section, we present the numerical results, according to the initial and perturbed conditions which we have prescribed (as shown in Figure III.2).

2.1 Case I. Continuum Shear Motion and $\beta_0^0 = 1.54$

Figure III.3 shows the evolution of the magnetic field lines (Figures III.3a, III.3b, and III.3c) and of the current intensity (Figures III.3d, III.3e, and III.3f). Figures III.3d, III.3e, and III.3f show a build-up in current intensity to 1457 Amp/km^2 (i.e. ~1.46 x 10^{-7} Amp/cm^2) at 2500 s after the shear is introduced. This corresponds to a shear angle of ~30° (Figure III.13) and the magnetic field strength being enhanced by a factor of 3. It can be seen in Figures III.3a, III.3b, and III.3c that some of the magnetic field lines are being pushed toward the neutral line, resulting in high current intensity. On the other hand, the outer magnetic field lines are shown locally opened up, due to the high pressure region being formed in that

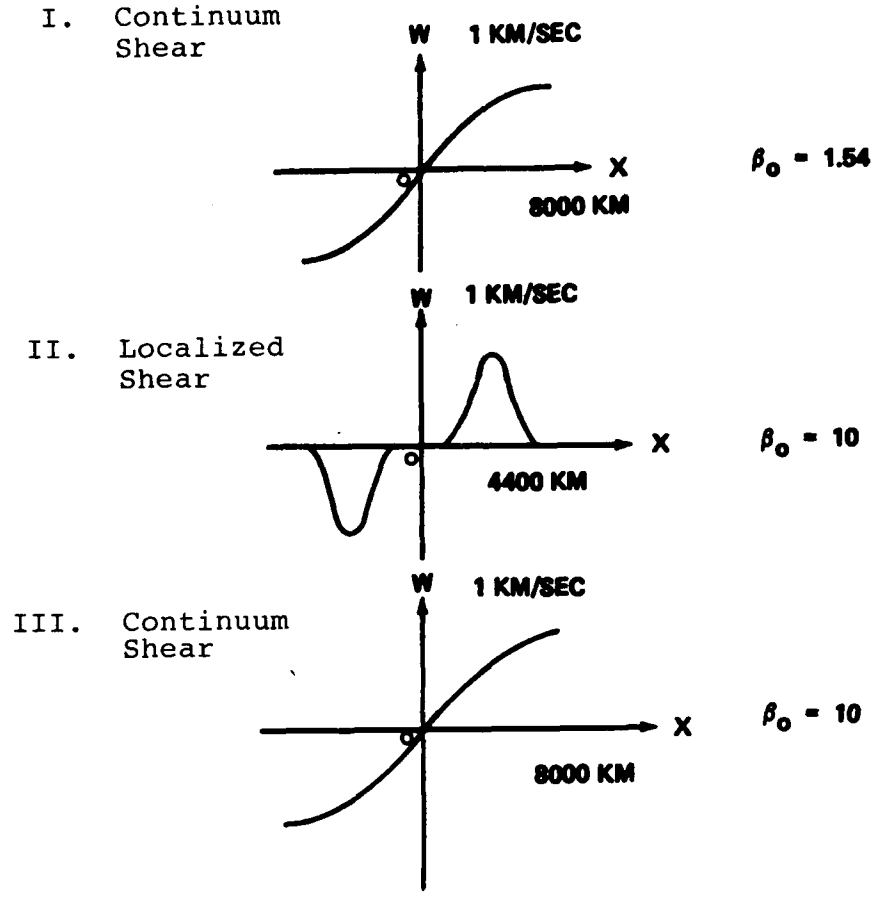

FIGURE III.2. Schematic Representation of the Prescribed Perturbations, i.e., the Configuration of Shear Motion Input to the MHD Model for a Specified Initial β_o.

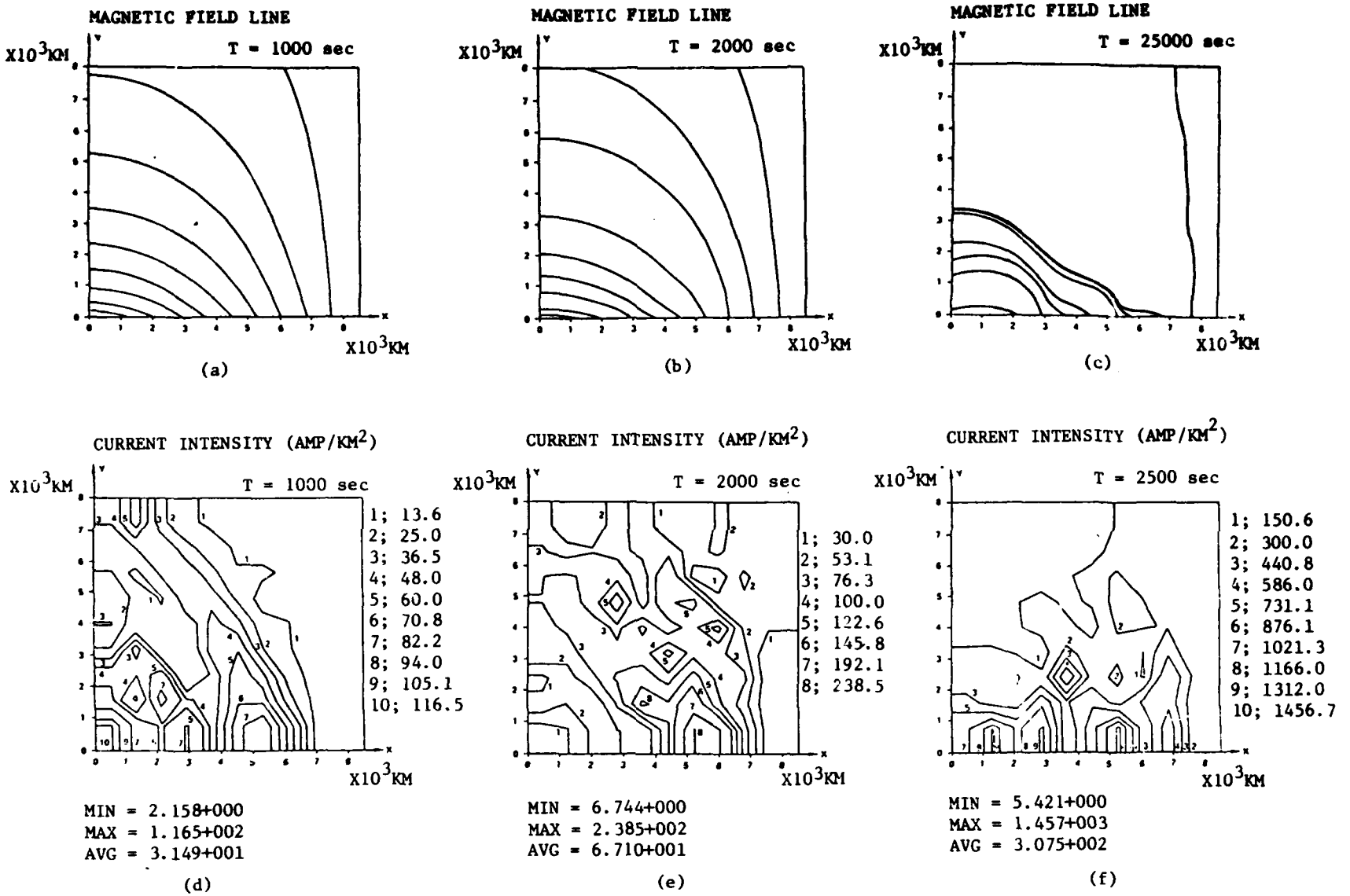

FIGURE III.3. The Evolution of Magnetic Field Configuration and Current Density Contours for Case I. The Continuum Shear and β_0^0 = 1.54 as Shown in Figure III.2. The minimum, maximum and average values are direct output from the computation and may not show up on the figure because of the lack of resolution.

region as shown in Figure III.5d, e, and f. But, it develops into a hill and valley type structure in the later time which may lead to irregular type of plasma flow such that turbulence may set in.

The plasma parameters (i.e. density and temperature) due to this perturbation are shown in Figure III.4. The density and temperature enhancement contours are due to this perturbation at 1000 s, 2000 s, and 2500 s, and are depicted in Figures III.4a, III.4b, III.4c, III.4d, III.4e, and III.4f, respectively. The pressure enhancement contours calculated for 1000 s, 2000 s, and 2500 s are shown in Figures 5d, 5e, and 5f, respectively. Because pressure is proportional to emission measure thus the high pressure region indicates high emission measures. From consideration of these induced plasma properties, we may draw the following conclusions:

(i) The density and temperature contours at 1000 s and 2000 s (Figures III.4a, III.4b, III.4d, and III.3e) clearly indicate a structured (non-homogeneous) loop-like shaped density enhancement (~10%) as shown by contour Number 5, with temperature being the order of 9×10^4 K, rising from the photosphere. Further this loop has a bright core at the top and near the leg as indicated by contours 6, 7 and 8. Based on the spectral characteristics, it should be observable in the H_α line. At 2500 s, this evolved into a more diffuse, cloud-like structure (density enhanced by ~40% and temperature ~6×10^4 K) moving outward to the corona.

(ii) It could also be noted that the largest density enhancement is at the leg and the next largest density

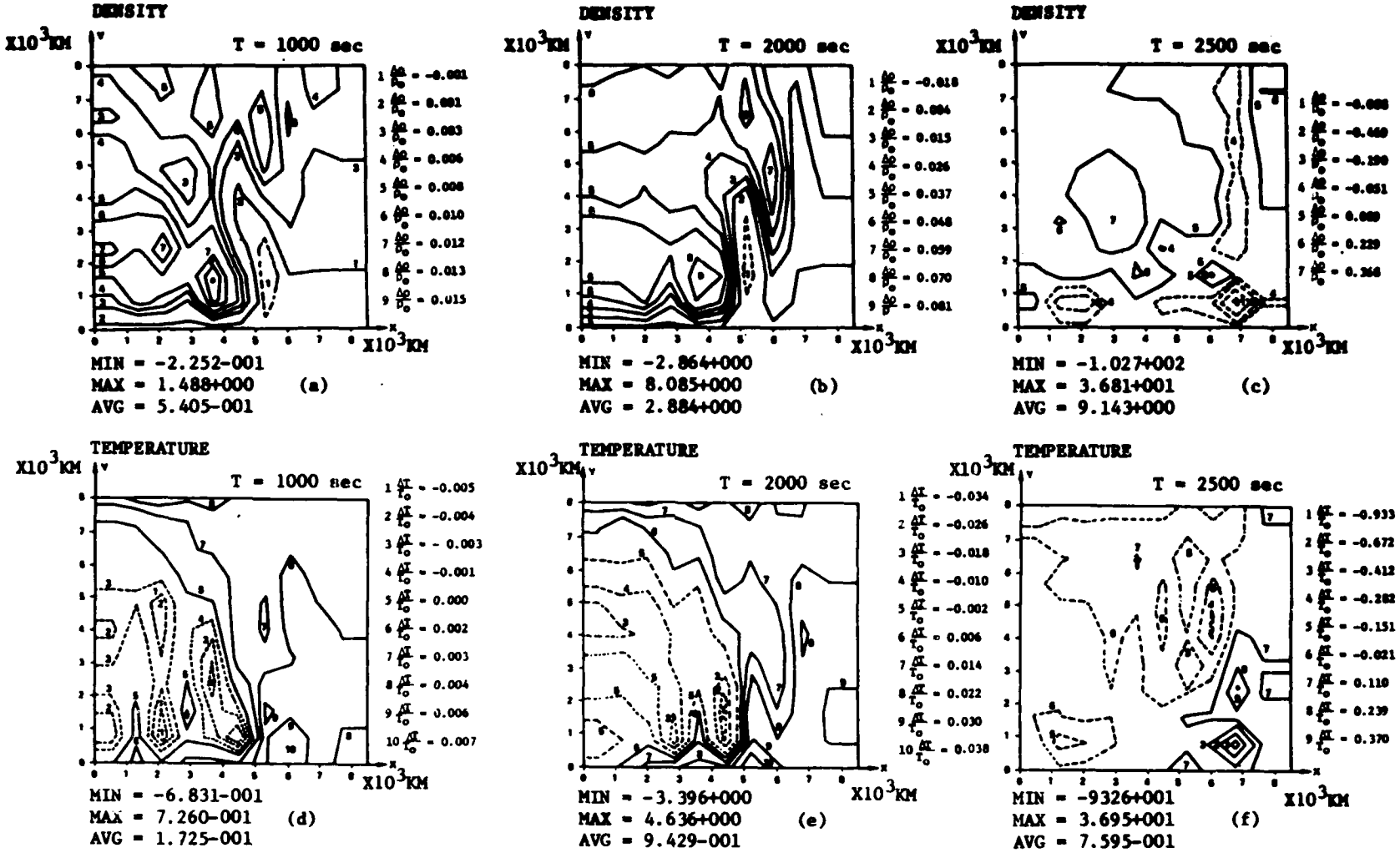

FIGURE III.4. Evolution of Solar Plasma Parameters (i.e. Density and Temperature) for Case I, the Continuum Shear and $\beta_0^0 = 1.54$ as shown in Figure III.2. The loops and patches are indicated by the heavy lines.

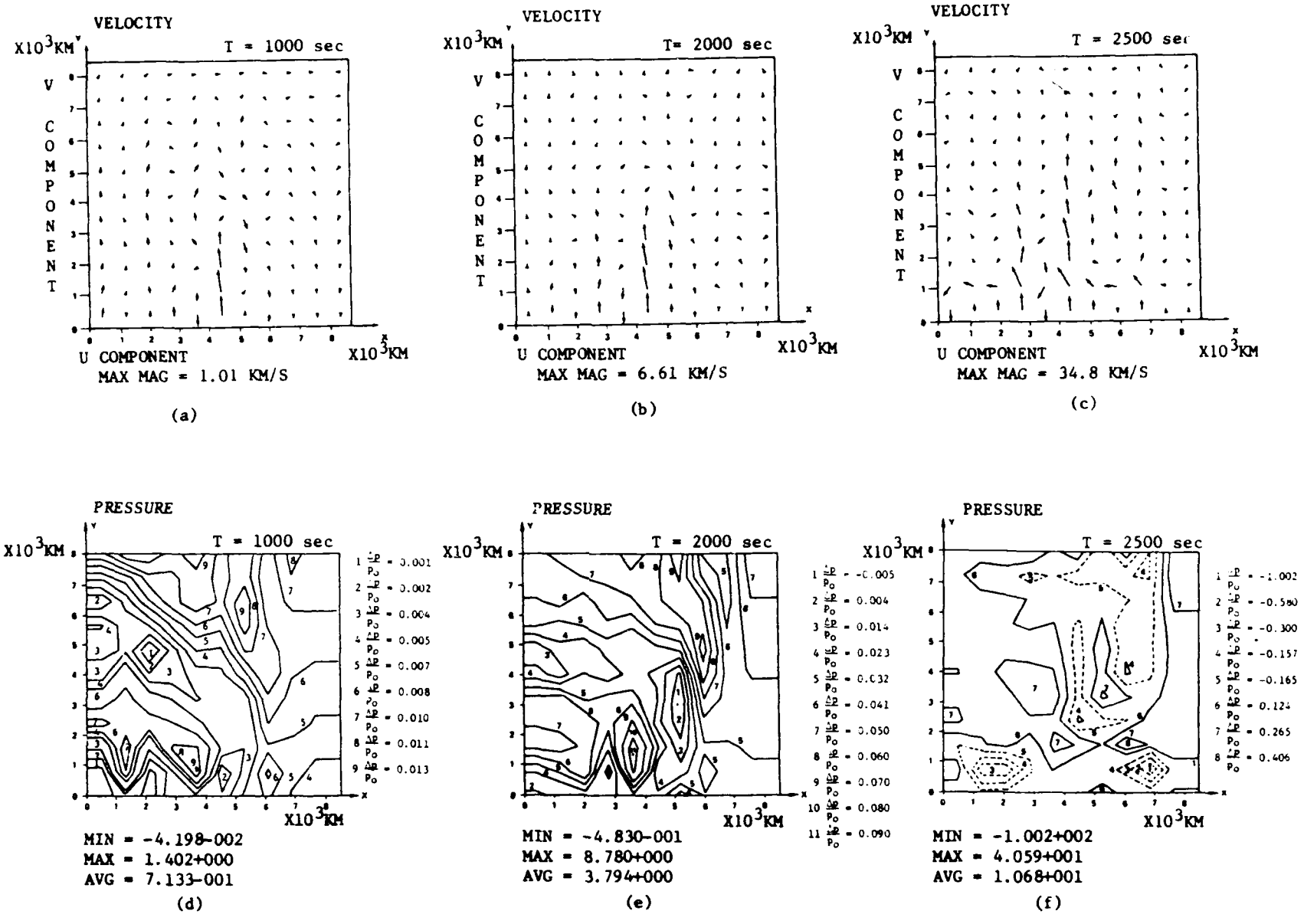

FIGURE III.5. Evolution of the Vectoral Representation of the Induced Velocity and the Pressure Contours for Case I, the Continuum Shear.

enhancement is at the leg and the next largest density enhancement is at the top. These structures can be interpreted as a loop, with the brightest part at the leg and the next brightest part at the top, with some faint structure in between. From these results, we can also estimate the size of the loop as being ~10^4 km in length and ~4 x 10^3 km in height by identifying the loop as the density contour 5 from the Figure III.4a, b.

Finally, the vectoral representation of the local velocity field at 1000 s, 2000 s, and 2500 s, respectively, is shown in Figures III.5a, III.5b, and III.5c. The purpose is to show the dynamical effects. There are two kinds of dynamical effects, one is the mass motion and the other is the wave motion. The mass motion is confined within the magnetic loop and fast mode of wave motion is propagation everywhere. The slow mode of wave is limited in a neighborhood along the field lines. This quantity has been shown to have an effect on the MHD dynamical instaility in relation to the mass ejection with a magnetic flux loop (Song, Wu and Dryer, 1987).

2.2 Case II. Localized Shear Motion and $\beta_0^0 = 10$

In order to examine the effects due to the strength of the magnetic field and configuration of the shear motion, we have performed a numerical test by using the shear motion, as shown in Figure III.2b and $\beta_0^0 = 10$. We first notice that, because the characteristic time is longer (this time is proportional to β_0^0), a long time is required to achieve asymptotic results.

Figure III.6 shows the evolution of the magnetic field lines (III.6a, III.6b, III.6c, and III.6d) and induced current

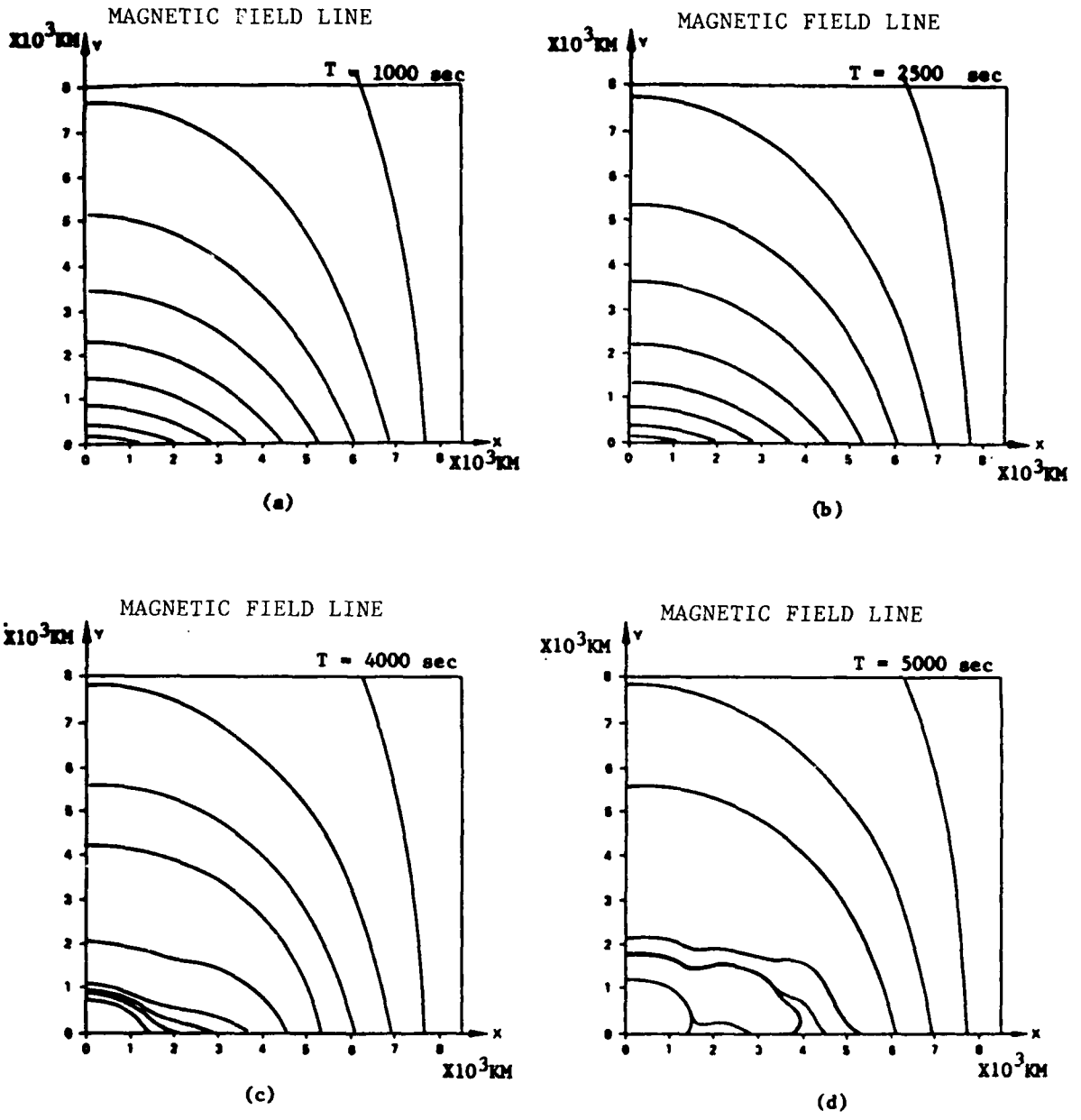

FIGURE III.6. Evolution of Magnetic Field Configuration for Case II, localized shear and $\beta_0^0 = 10$.

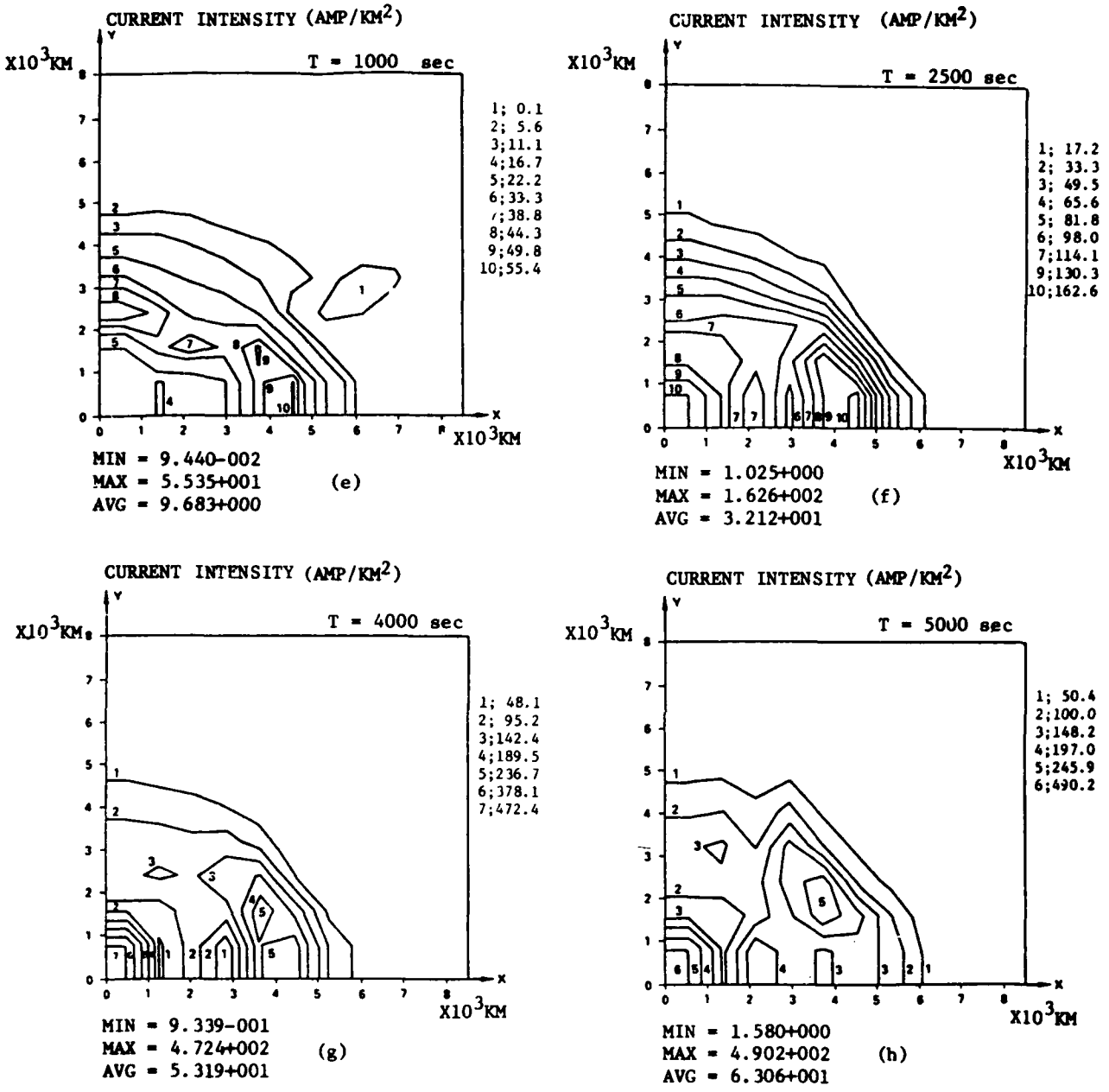

FIGURE III.6. Evolution of Current Intensity Distribution for Case II, localized shear and and $\beta_0^0 = 10$.

intensity contours (III.6e, III.6f, III.6g, and III.6h) at 1000 s, 2000 s, 4000 s, and 5000 s after introduction of the perturbation. We observe that the highest induced current intensity is 500 Amp/km^2 (i.e. 5 x 10^{-8} Amp/cm^2) in the neighborhood of the top of these neutral lines. Also it is worthy to notice that the magnetic field lines have orderly changes up to 4000 s, then, we observed that some of the field lines coelesence together forming high intensity current sheets as indicated in Figure III6.d.

Figure III.7 shows the disturbed plasma properties: density enhancement contours (III.7a, III.7b, III.7c, and III.7d), temperature enhancement contours (III.7e, III.7f, III.7g, and III.7h), and pressure contours (III.8e, III.8f, III.8g, and III.7h) at 1000 s, 2500 s, 4000 s, and 5000 s, respectively. The maximum density enhancement has reached a factor of ~8, with temperature enhancement being 0.07% (i.e.~ 2 x 10^5 k), and the value of density depletion is a factor of 2, with the temperature being lowered by 130%. Since this is an ideal MHD calculation, the physical mechanism causes this cooling is adiabatic cooling. These plasma properties should produce UV and H_α emission enhancements. It can further be noticed that by inferring the density countour the initial structure shown in Figure III.7,a, b, c has a loop shape with a bright leg (i.e. up to 4000 s), and breaks into bright patches when the time reaches 5000 s. This may indicate that some kind of instability has occurred, as can be seen from the vectoral representation of velocity evolution shown in Figure III.8a, b, c and d. Figure III.8e, f, g and h

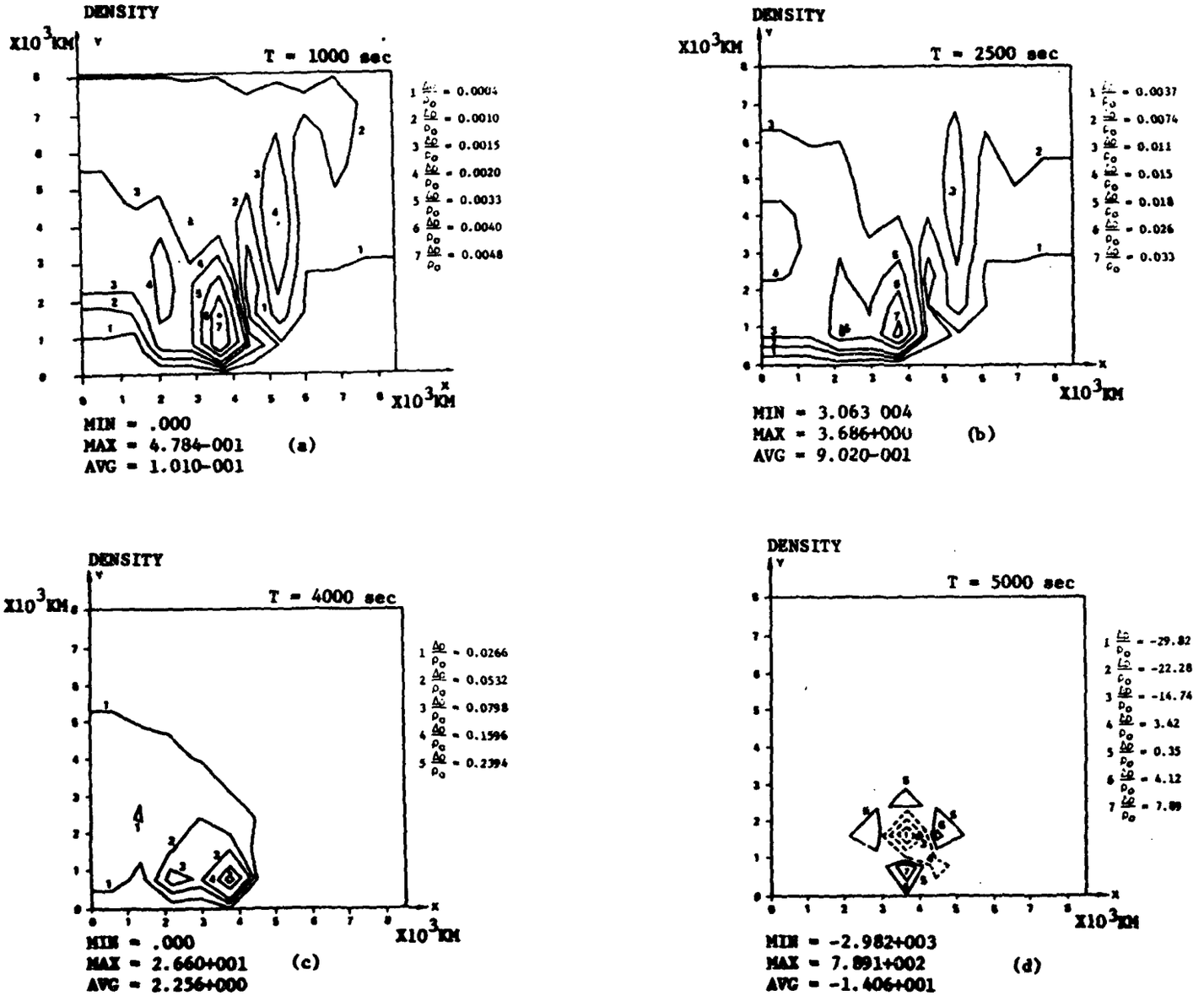

FIGURE III.7. Evolution of the Density Contours for Case II, localized shear and $\theta_0^0 = 10$.

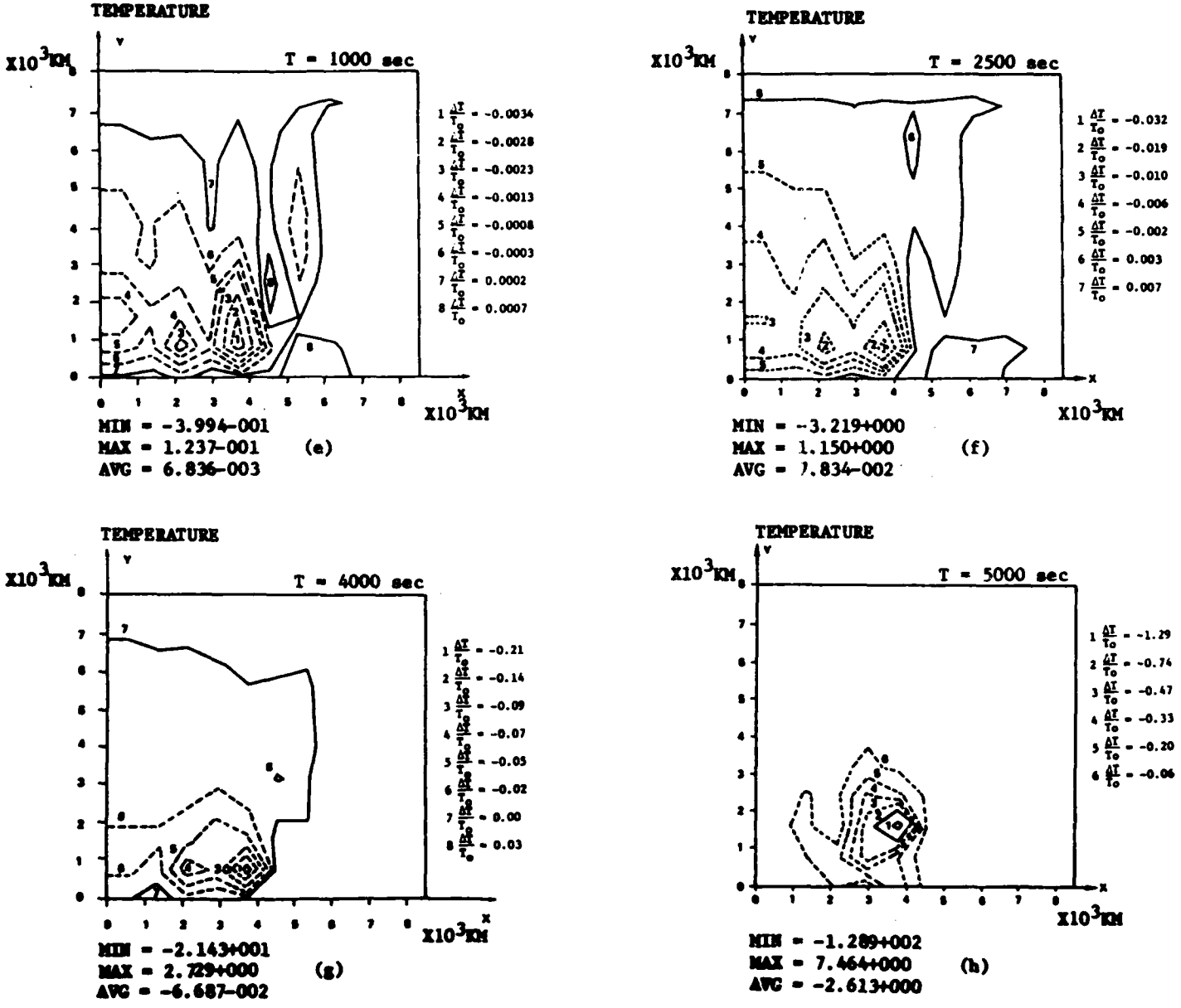

Figure III.7. Evolution of the Temperature for Case II, localized shear and $\beta_0^0 = 10$

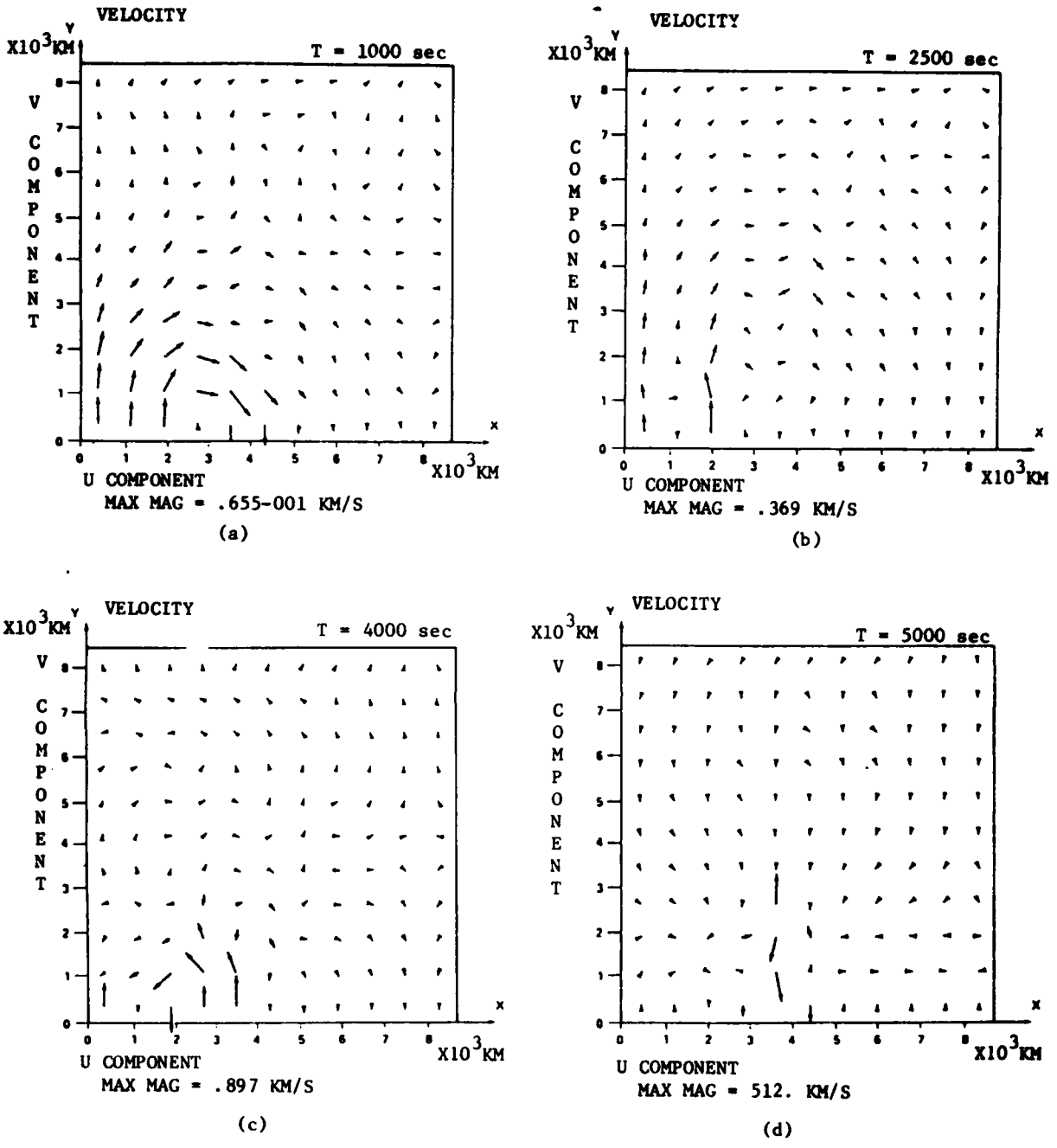

FIGURE III.8. Evolution of the Vectoral Representative on the Velocity Distribution for Case II, Localized Shear Motion and $\beta_0^0 = 10$

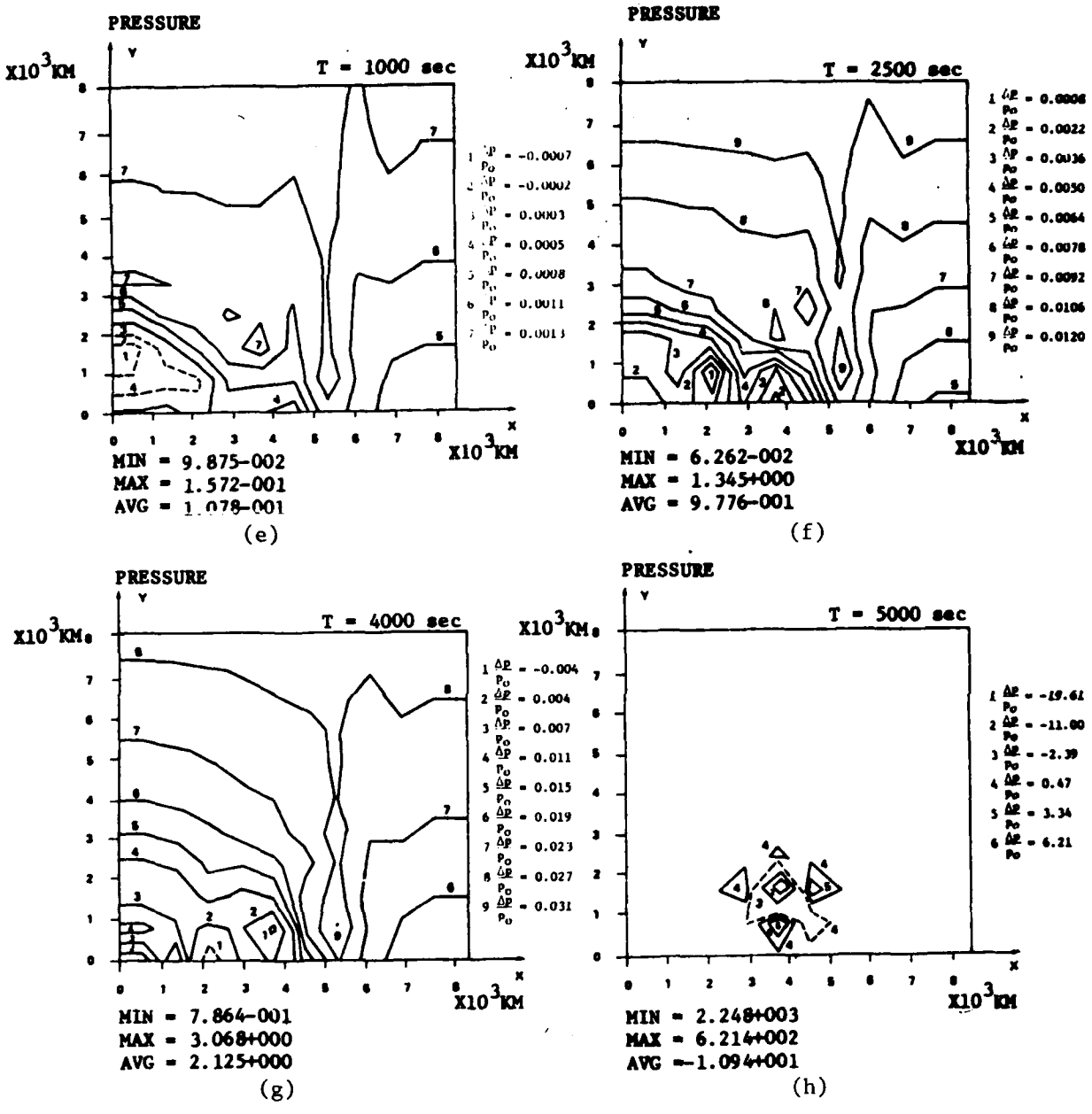

Figure III.8. Evolution of Pressure Contours for Case II, Localized Shear Motion and $\beta_0^0 = 10$

exhibit the pressure evolution of an active region. From these results, we may note that, initially, the motion is very regular, but as the time progresses, the irregular motion is developed. However, we cannot conclude whether this is turbulence or MHD instability since a detailed analysis could not be made, due to the compultational limitation in spatial resolution (i.e. order of arc second to allow us to determine the plasma turbulence).

2.3 Case III. Continuum Shear Motion and $\beta_0^0 = 10$

In order to investigate the effects due to the initial value of the plasma and configuration of the shear, we have chosen this case for comparison with case I (for showing the initial plasma beta (β_0^0) effects) and with case II (for showing the effects due to shear configuration).

Figure III.9 shows the evolution of the magnetic field and induced current intensity. In comparing these results with Figures III.3 and III.6, the effects due to β_0^0 and shear configuration are interpreted as follows:

(i) In comparing Figures 3a-3d with Figures III.9a-9d, we note that the deformed magnetic field line takes a longer time to reach the asymtotic state. Physically, this occurs because the characteristic time scale is proportional to the β_0^0. Further, it also could be interpreted that the weak field strength is easily deformed.

(ii) The induced current intensity is inversely proportional to β_0^0. For example, the maximum induced current intensity is ~300 Amp/Km^2 for $\beta_0^0 = 10$ at 4000 s and is 1500 Amp/km^2 for $\beta_0^0 = 1.54$ at 2500 s. This means that the electrical

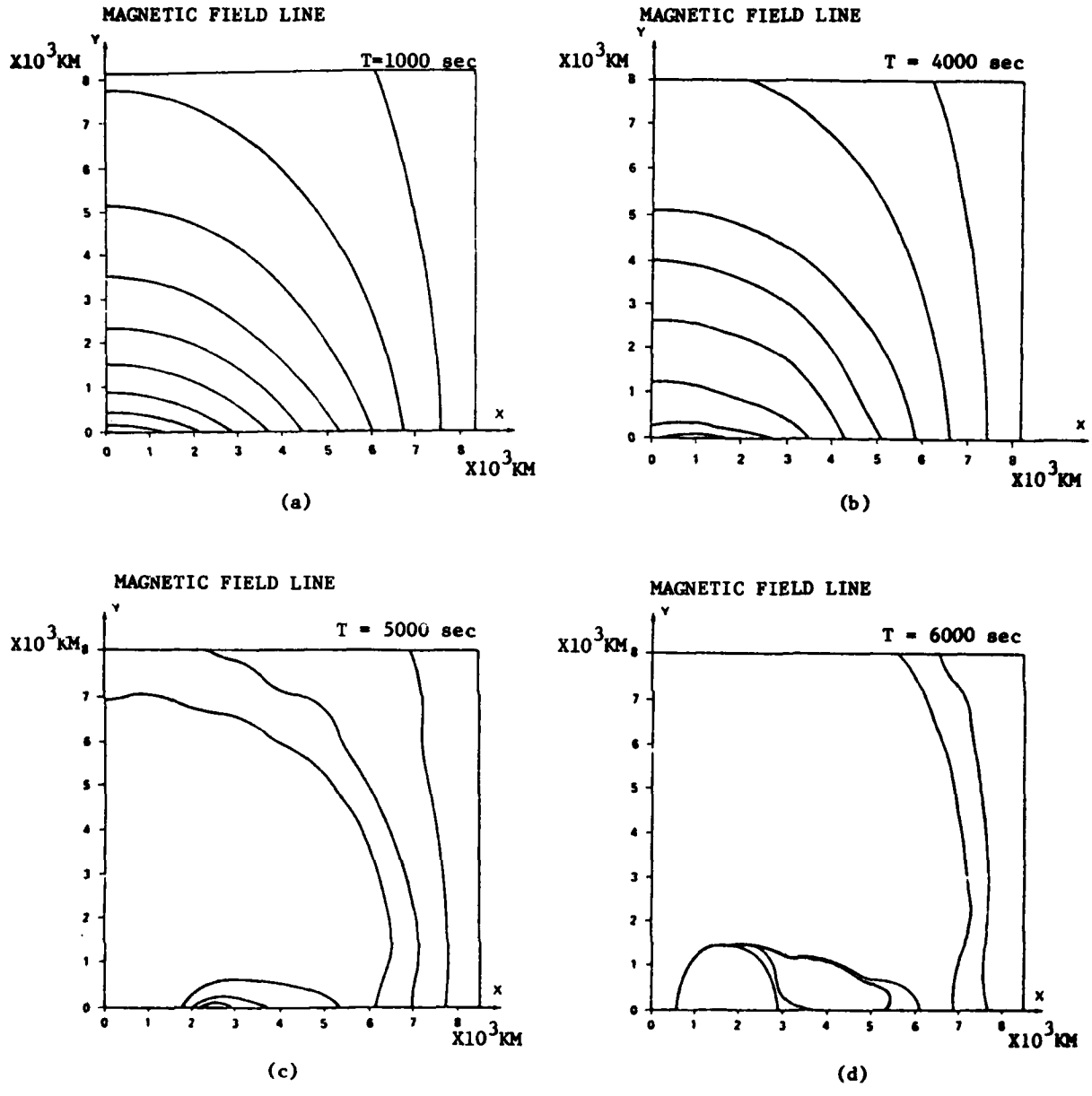

FIGURE III.9. Evolution of Magnetic Field Configuration of an Active Region for Case III, Continuum Shear and $\beta_0^0 = 10$.

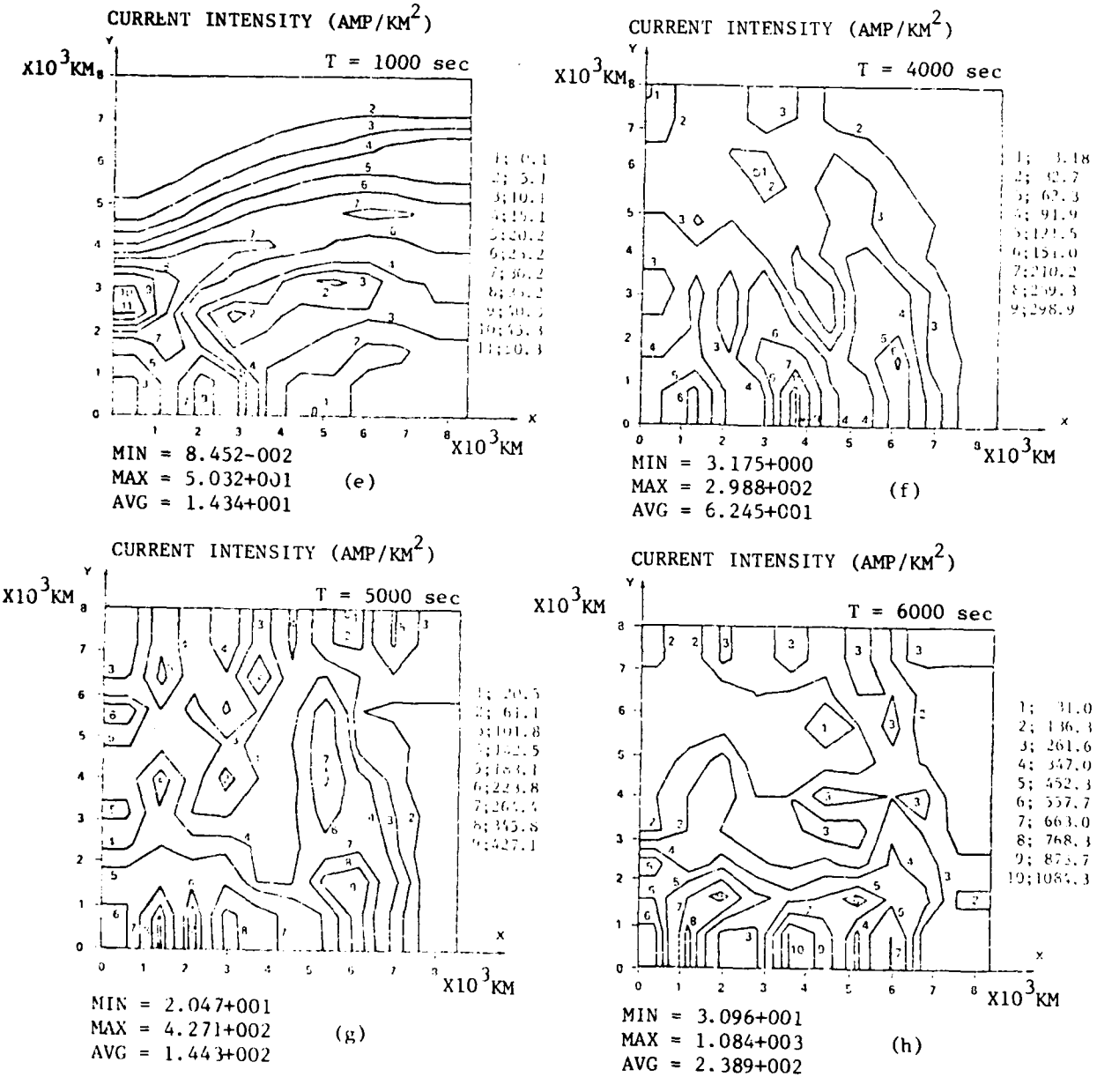

FIGURE III.9. Evolution of Current Intensity Contours for Case III, Continuum Shear Motion and $\beta_0^0 = 10$

current build-up due to shear is much faster and larger in the case of high magnetic stress region.

(iii) The different shear configuration resulted in the different location of the maximum induced current. For the locally sheared case, the maximum induced current is located farther away from the neutral line, where there is greater shear. The magnitude of induced current intensity is practically the same for the two cases (i.e. Case II and III), since they have the same magnetic field strength. Physically this implies that the movement of sunspots has the effects on the location of the occurance of the flare.

Figure III.10 shows the density and temperature contours for the disturbed plasma, due to the continuum shear motion for β_0^0, at 1000 s, 4000 s, 5000 s, and 6000 s, respectively. From these results, the maximum density and temperature enhancements are also shown to be proportional to the β_0^0. This is physically obvious, because the stronger field produces stronger wave compression, and leads to higher density and temperature enhancements. Finally, we show the pressure and vectoral representation of the velocity distribution at 1000 s, 4000 s, 5000 s, and 6000 s, respectively (Figure III.11). Again, the circular motion from the neutral line to the right (i.e. away from the neutral line; Figure III.11) is exhibited. The velocities become more randomly distributed at a later time.

Figure III.12 shows maximum current intensity build-up as a function of time for the three different cases. By consideration of these calculated results, the following interesting physical

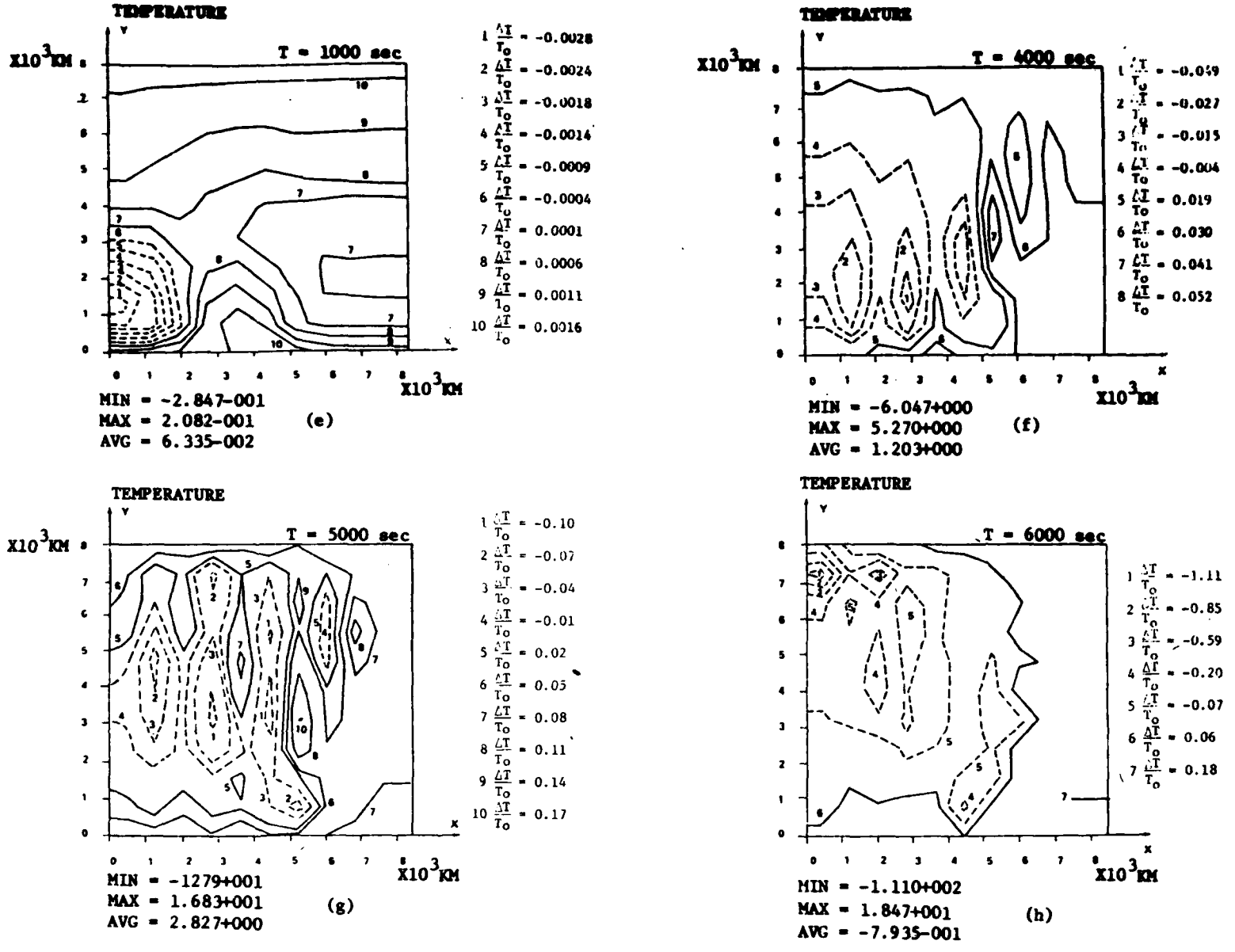

FIGURE III.10. Evolution of Temperature Distribution for Case III, Continuum Shear and $\beta_0^0 = 10$.

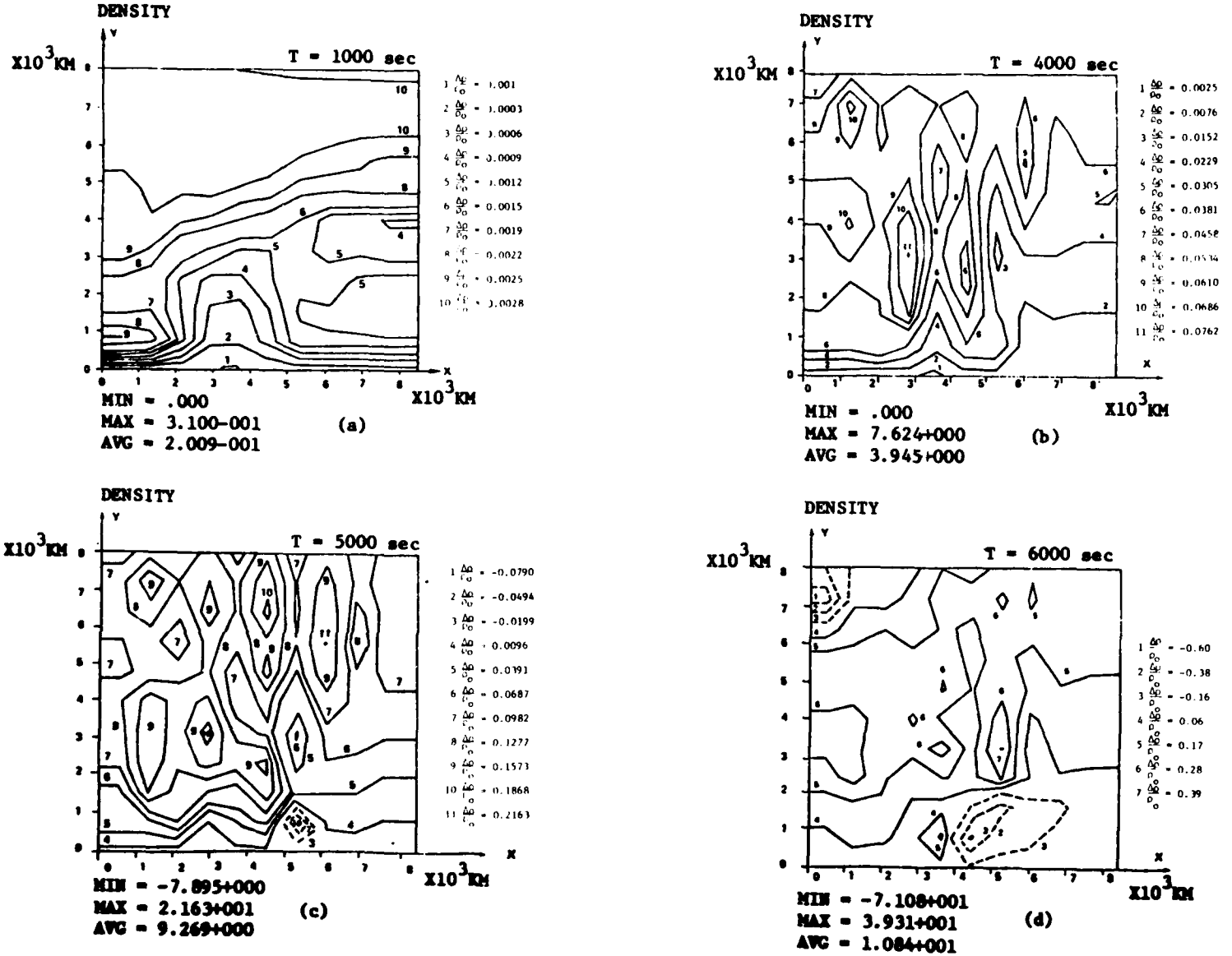

FIGURE III.10. Evolution of the Density Contours for Case III, localized shear and $\beta_0^0 = 10$.

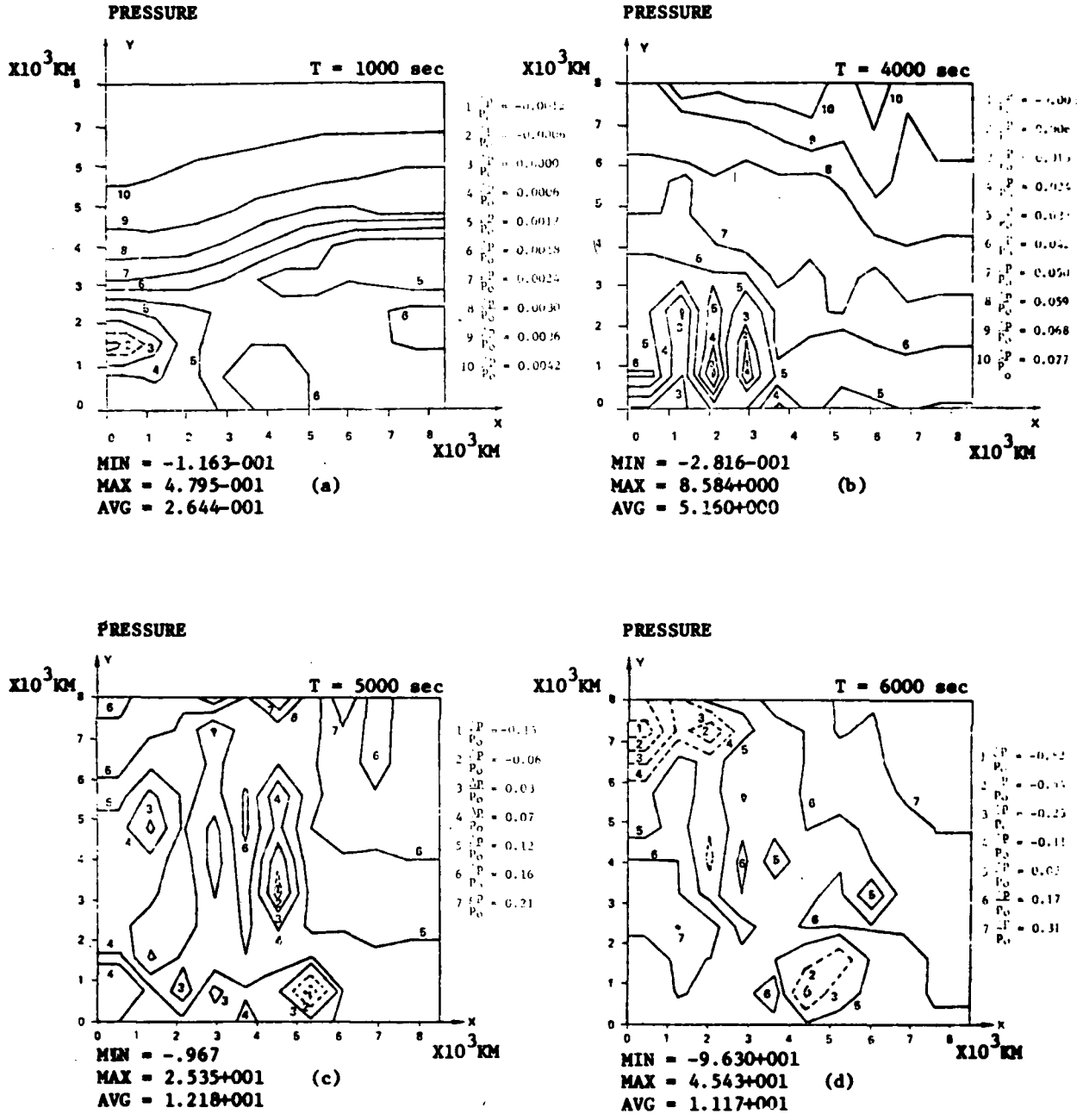

FIGURE III.11. Evolution of Pressure Distribution of an Active Region for Case III, Continuum Shear and $\beta_0^0 = 10$.

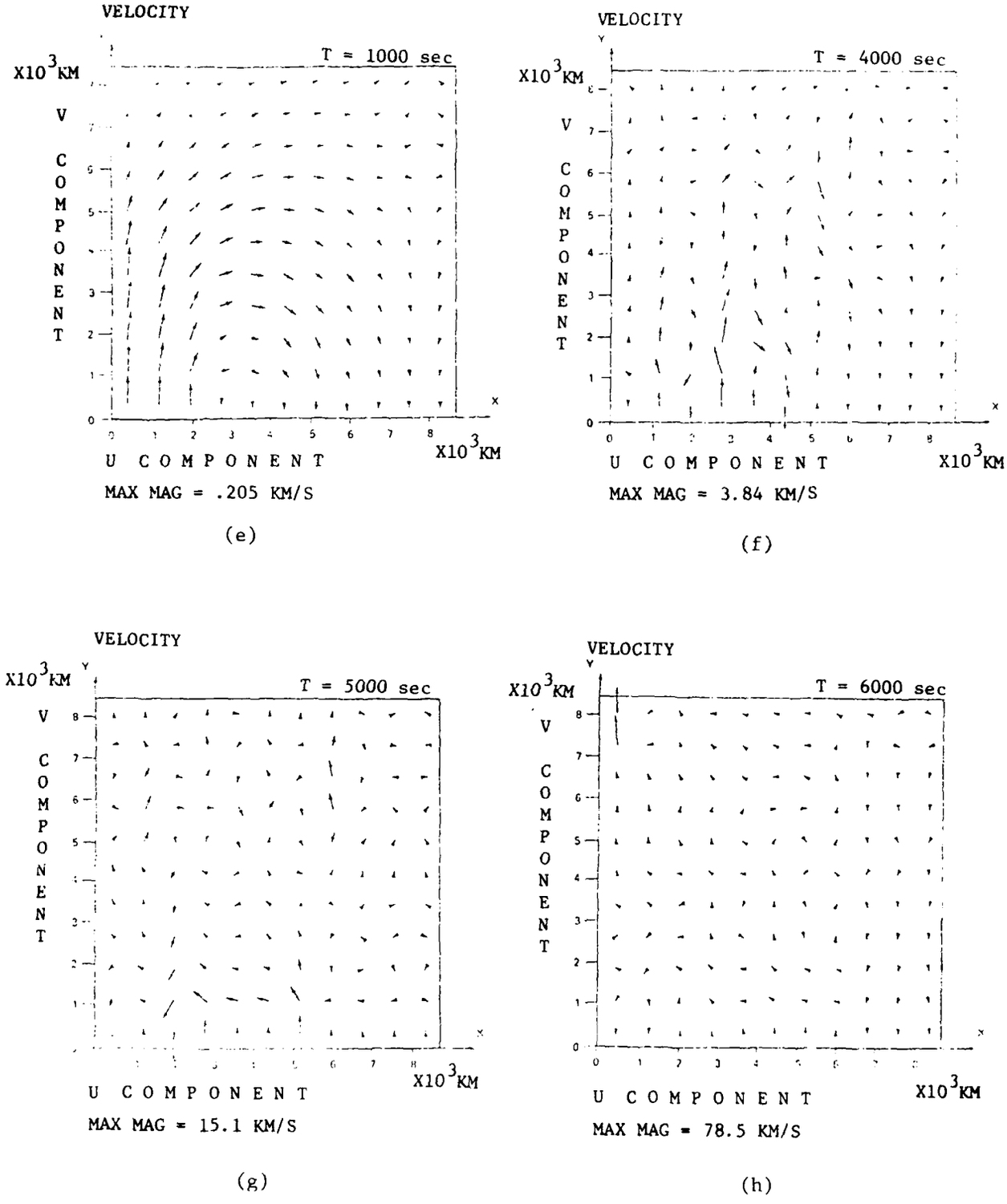

FIGURE III.11. Evolution of Velocity of an Active Region for Case III, Continuum Shear and $\beta_0 = 10$.

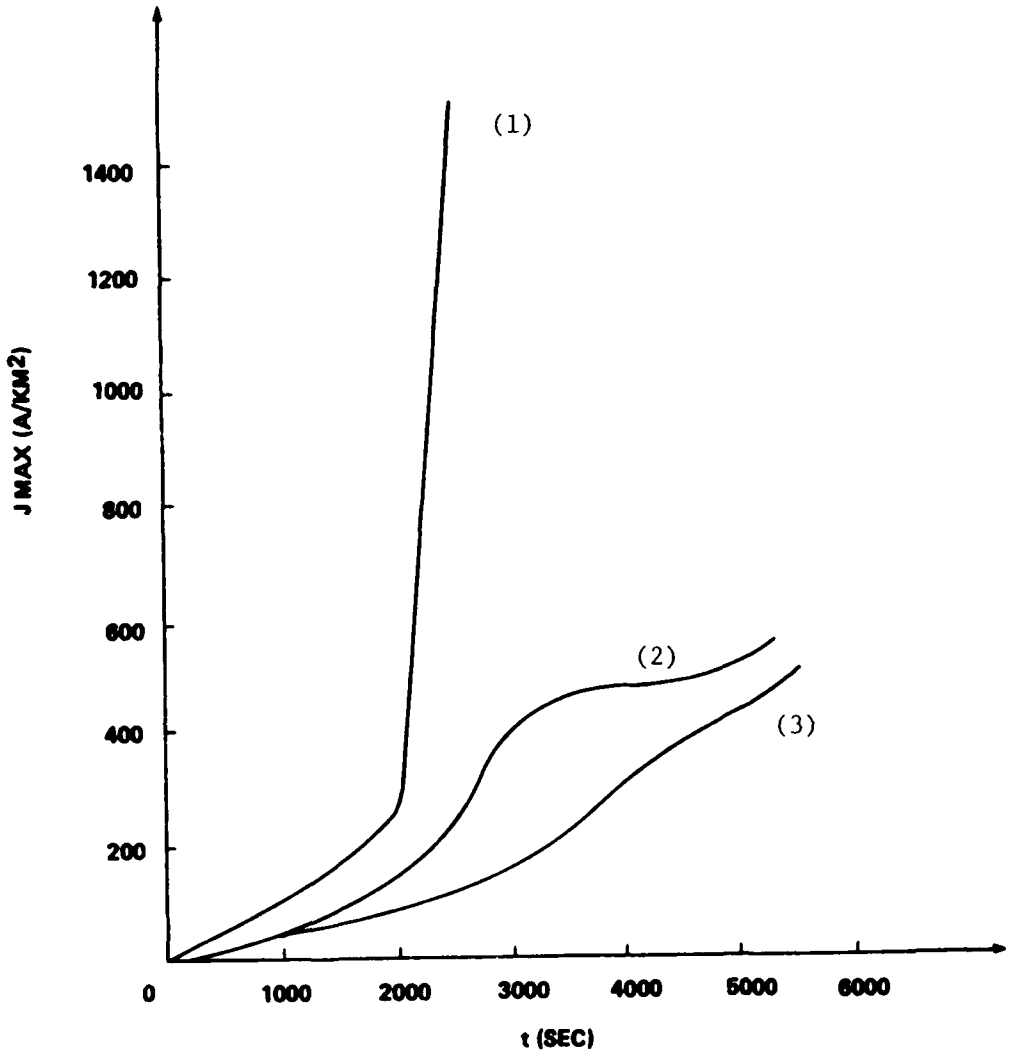

FIGURE III.12. Maximum Current Density of an Active Region VS Time for Three Different Cases as Shown in Figure III.2.

results are revealed:

(i) The growth rate of current is proportional to initial field strength.

(ii) The localized shear produces a large local maximum current at a particular position and a specific time, when this current dissipates, it will result in a flare at this particular position. Thus we may suggest a scenario that the photospheric shear motion will increase the twists of the magnetic field lines, such that, the local current intensity increases. Simultaneously, the plasma flow becomes irregular as shown in Figures III.5, 8, and 11. With these increased dynamical effects, it may enhance the resistivity, the current can be dissipated efficiently which supplies the energy for flaring.

Figure III.13 shows the shear angle distribution view from the top versus the height at various times, as the shear motion is introduced at lower boundary for these three cases. Actually this is one of the computed physical parameters which could be connected with the observation. We shall elaborate this point in Section IV. From these results we may note:

(i) The initial photospheric velocity shear configuration affects the field shear angle distribution significantly. For example, the largest shear angle always exists in the lower atmosphere for locally sheared motion.

(ii) By comparison with Case I and III, the results showed the influence of initial field strength (i.e. β_0^0) on the shear angle distribution. The shear angle is almost constant with respect to height for the stronger initial field strength. On

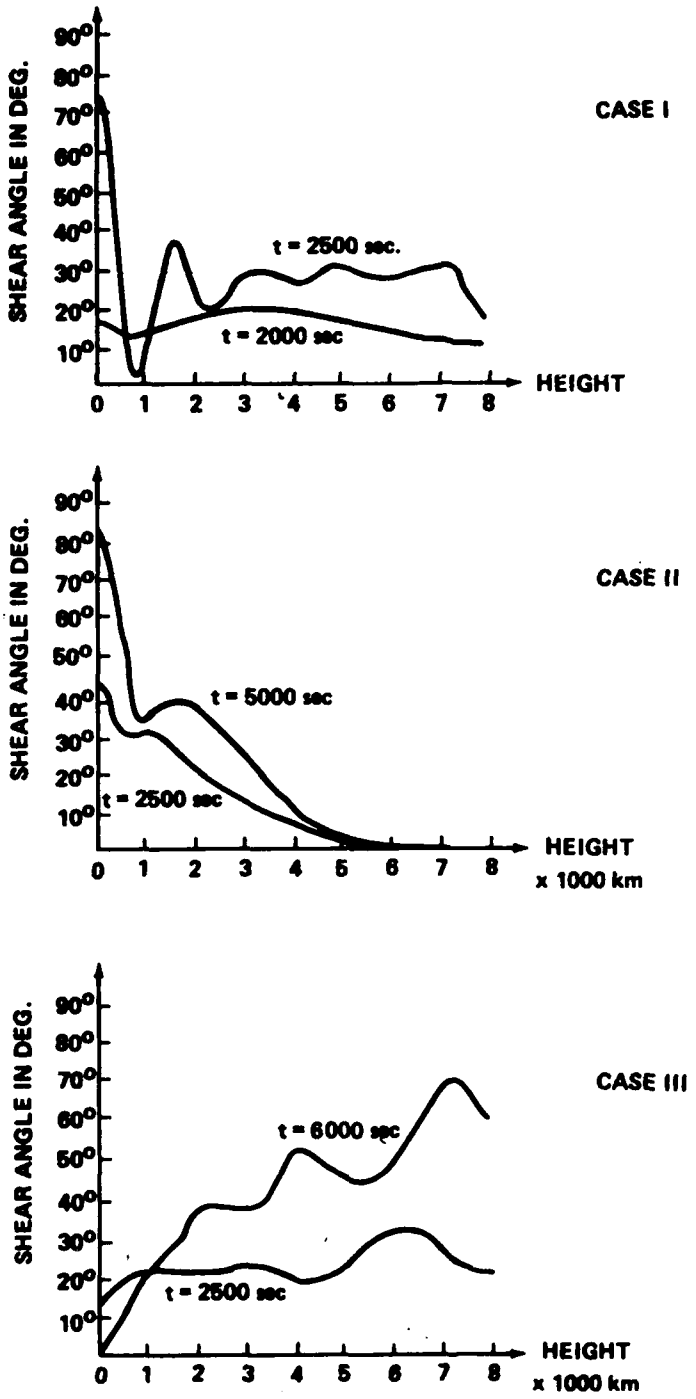

FIGURE III.13. Shear Angle Distribution projected on x-z plane at various Height at Various Times for These Three Cases as Shown in Figure III.2.

the other hand, the largest shear angle appeared in the higher atmosphere with initially weak field strength.

The larger shear angle means higher twist of the local magnetic field, which is an indication of the locally higher magnetic field gradient. Considerable significance can be drawn from this result because the magnetohydrodynamic (MHD) theory implies that larger localized magnetic field gradient will enhance the MHD instability such that flare is triggered. Thus, we may suggest the site of the flare will depend on the photospheric velocity shear configurations and initial magnetic field strength, which shows the velocity shear angle being a function of these two parameters as shown in Figure III.13. In short, what we suggest here is that using field gradient as a measured quantity for flare prediction. Because we could not make such a measurement in the meantime, we have shown from the model calculation that the field gradient is related to shear angle and the shear angle depends on initial field strength and velocity shear configuration in which these parameters can be deduced from SOON's data.

3. Physical Interpretation of Numerical Results

In this section, we shall utilize these computer-simulated results to investigate physical characteristics related to the occurrance of the solar flare. The important physical characteristics related to the solar flare are: (i) available energy, (ii) magnetohydrodynamic instability in relation to the triggering mechanism of a solar flare, and (iii) the energy-release time-scale of a solar flare. We shall discuss these

parameters, based on this numerical simulation model, in some detail, as follows:

3.1 Availability of Magnetic Energy

Based on these three simulation cases, the computed maximum local excess magnetic energy density growth rate $\left(\frac{dE_m}{dt}\right)_{max}$ at a specific time and location after the introduction of shearing motion are presented in Table III-1. In these computations, we terminate our computation when the computed parameters become linear function of time. Thus, we are able to estimate the total energy resulting from a prescribed photospheric shear motion by simply multiplyinig time with the magnetic energy growth rate. For example, a typical buildup time for an active region is an order of a few days. Therefore, we obtained the following:

Excess Magnetic Energy (ΔE_m) erg/km^3

	1 day (86,400 s)	2 days (172,800 s)	3 days (259,200 s)	4 days (345,600 s)
CASE I	1.4×10^{20}	2.8×10^{20}	4.2×10^{20}	5.6×10^{20}
CASE II	2.16×10^{19}	4.32×10^{19}	6.48×10^{19}	8.64×10^{19}
CASE III	3.46×10^{18}	6.92×10^{18}	1.04×10^{19}	1.38×10^{19}

In this simulation, the computational domain is $1.6 \times 10^4 \times 1.6 \times 10^4 \times 8 \times 10^3$ km ^{3} (i.e. $\sim 2.05 \times 10^{12}$ km^3), thus, the total magnetic energy stored in the active region is in the range of $10^{30} - 10^{32}$ ergs for one day and $10^{31} - 10^{33}$ ergs for four days. This indicated that there is enough energy to supply flaring. How this stored energy can be released - we suggest that it will depend on the MHD instability - is addressed in the next section.

TABLE III.1

Maximum Magnetic Energy Growth Rate

Time	2500 sec	2500 sec	2500 sec
Case	$\left(\frac{dE_m}{dt}\right)_{max}$ erg/(km)^3 sec.	$\left(\frac{dE_m}{dt}\right)_{max}$ erg/(km)^3 sec.	$\left(\frac{dE_m}{dt}\right)_{max}$ erg/(km)^3 sec.
I	1.6×10^{15}		
II	2.3×10^{12}	2.5×10^{14}	
III	3.9×10^{11}	1.3×10^{13}	4×10^{13}

E_m : Magnetic Energy Density
max: Maximum Value in the Calculation Domain

3.2 Magnetohydrodynamic (MHD) Instability

Now, we shall examine whether the computed physical system is subject to magnetohydrodynamic (MHD) instability. In order to perform a simple MHD instability analysis estimation, we shall use the principle of tearing mode MHD instability (Tachi et al., 1983 and Van Hoven, 1980) to test our computed results. Tachi et al. (1983) have concluded that if the magnetic Reynolds number, $Re_M = 10^{-2}\ aBT^{3/2}n^{-1/2}$, exceeds 3×10^5, both tearing mode and joule heating mode are possible for $\alpha = ka = 0.1$ with k being the wave number of the perturbation and "a" is the characteristic length. In our model calculation, we have:

$B_0^0 \simeq 10 \sim 20$ Gauss,

$T \simeq 10^5$ K,

$n \simeq 10^{12}$ cm^{-3},

and the shear motion is prescribed in the form of $\sin\left(\frac{\pi x}{x_0}\right)$. The x_0 is the horizontal length of the computation domain, we have chosen to be 8×10^8 cm, therefore, the wave number of the perturbation k is equal to $\pi/x_0 = 3.1416/8 \times 10^8 \sim 4 \times 10^{-9}$ cm^{-1}. With this information, the magnetic Reynolds number for the present model can be computed from

$$Re_M = 10^{-2}\ \frac{\alpha}{k}\ \frac{BT^{3/2}}{n^{1/2}}$$

$$= 10^{-2}\ \frac{\pi}{k}\ \frac{BT^{3/2}}{n^{1/2}}$$

$$= 10^{-2} \frac{0.1}{4 \times 10^{-9}} \frac{20 \times (10^5)^{3/2}}{(10^{12})^{1/2}}$$

$$= 1.58 \times 10^8$$

This value is much larger than the value (3×10^5) given by Tachi et al., (1983) for triggering both tearing mode and joule heating mode. Namely, these computed cases in the present study will lead to MHD instabilities. Thus, energy relaease is possible. Now, the next question is whether the time scale of energy release is appropriate for a flare? This will be discussed in the following section.

3.3. Time-Scale of Energy Release

Let us choose the physical mechanism for the energy release as due to "joule dissipation." This choice is made because the computed results for the magnetic Reynolds number indicate that both tearing mode and joule heating mode instability are possible. It is known, that the time scale for the energy release predominately depends on the resistivity "η". Since the present simulation model has only included the effects of joule dissipation, not the tearing mode instability, we shall only employ joule heating mode for this analysis. In order to estimate the energy release time, we have depicted the energy dissipation rate in Table III-2 for the three cases being investigated. These results are highly dependent on the resistivity. Three different kinds of resistivity are investigated;

a) Classical resistivity (i.e., Spitzer resistivity)

$$\eta_s = 1.30 \times 10^{-9} \frac{Z \ln\Lambda}{T^{3/2}} \quad s^{-1} \qquad (9)$$

TABLE III.2

Computed Maximum Energy Dissipation Rate for Various Resistivities and Various Different Initial Values of β_o As Well As Configuration of Shear Motions at a Specific Time

Time	2,500 s			
Case	$\vec{J}_{max}$ (A/km^2)	$\eta_s J^2_{max}$ (erg/km^3-s)	$\tilde{\eta}_\perp J^2_{max}$ (erg/km^3-s)	$\tilde{\eta}_\perp \vec{J}^2_{max}$ (erg/km^3-s)
I	1457	1.1×10^5	7.8×10^9	7.8×10^{14}
II	163	1.3×10^3	1.0×10^8	1.0×10^{13}
III	109	6.0×10^2	4.4×10^7	4.4×10^{12}

Time	5,000 s			
Case	$\vec{J}_{max}$ (A/km^2)	$\eta_s J^2_{max}$ (erg/km^3-s)	$\tilde{\eta}_\perp J^2_{max}$ (erg/km^3-s)	$\tilde{\eta}_\perp \vec{J}^2_{max}$ (erg/km^3-s)
I	-	-	-	-
II	490	1.2×10^4	8.9×10^8	8.9×10^{13}
III	132	8.7×10^2	6.4×10^{12}	6.4×10^{12}

Time	6,000 s			
Case	$\vec{J}_{max}$ A/km^2)	$\eta_s J^2_{max}$ (erg/km^3-s)	$\tilde{\eta}_\perp J^2_{max}$ (erg/km^3-s)	$\tilde{\eta}_\perp \vec{J}^2_{max}$ (erg/km^3-s)
I	-	-	-	-
II	-	-	-	-
III	325	5.3×10^3	3.9×10^8	3.9×10^{13}

where $\Lambda = \frac{3}{2Ze^3}\left|\frac{k^3T^3}{\pi\, n_e}\right|^{1/2}$, with Z being the atomic number, n_e the number density of electron, e, the electric charge, k the Boltzmann constnat and T the temperature. From the present simulation result, we found the shear motion induced density at the location of the maximum current is $\sim 10^{12} cm^{-3}$ and the temperature is $\sim 10^{5}{}^{\circ}K$. By substituting these values into Equation (9), it gives the classical resistivity to be $5.54 \times 10^{-16}\ s^{-1}$.

b) Classical resistivity with magnetic field effect. If we take into account the effect of the magnetic field, the resistivity will be classified into two parts; the resistivity parallel to the magnetic field,

$$\eta_{||} = \eta_s \tag{10}$$

and resistivity perpendicular to the magnetic field

$$\eta_{\perp} = \left[1 + \left(\omega_B/\nu_e\right)^2\right]\eta_{||} \tag{11}$$

with ω_B and ν_e being the cycletron and collision frequency, respectively and they are represented by

$$\left.\begin{aligned} \omega_B &= \frac{eB}{mc} \\ \nu_e &= \frac{12 n_e e^4}{(kT_e)^{3/2} m^{1/2}} \end{aligned}\right\} \tag{12}$$

where m, is the hydrogen mass, and B is the magnetic field strength. In the present analysis we

have: B = 20 G; T = 10^{5}°K; n_e = 10^{12} cm^{-3}, This gives us the $\eta_{||} = \eta_s = 5.54 \times 10^{-16}$s, and $\eta_{\perp} = 4.1 \times 10^{-11}$ s.

c) Anomalous Resistivity

Recently, Wu et al., (1987) have shown that when considering the soliton and strong Langmuir turbulent effects, the resistivity could increase several orders of magnitude (i.e., 10^4 ~ 10^5). Using these results given by Wu et al. (1988), the anamolous resistivity would be:

$$\bar{\eta}_{||} = 5.54 \times 10^{-11} \text{ s}$$

$$\bar{\eta}_{\perp} = 4.1 \times 10^{-6} \text{ s}$$

By employing these resistivities (i.e., by η_s, $\eta_{||}$, $\eta_{\perp}$, and $\bar{\eta}_{\perp}$) we have computed the energy dissipation rates as shown in Table III.2. From these computed results of three different case, we may make the following conclusions.

i) The only reasonable dissipation rate is the one with anomalous resistivity. From the results shown in Table III-2, it is obvious that the dissipation rates associated with classical parallel and perpendicular resistivities are too small to match the time-scale of a flare energy release. For example, the energy dissipation rate for Case I (i.e., the largest dissipation rate) is 7.8 x 10^{14} erg/km^3 - s.

Based on our computational domain, the physical volume is 10^{12} km^3. This gives a total energy dissipation rate of 7.8×10^{26} erg/s. If we consider a medium flare processing 10^{30} ergs, the time-scale of energy release becomes 1250 s (i.e., ~ 20 min) which matches a typical flare time.

ii) Also it could be noted that the smaller the plasma beta the larger the energy dissipation rate.

Finally, we should state, the joule dissipation is not a reasonable one. We merely chose this particular one for testing, which shows the joule dissipation mechanisms can be a candidate for flare energy release.

IV. Relationship Between the Observations and Simulation Model

In this section, an example is used to illustrate the relationship between the observations and the simulation model output in the prediction of solar flares. Followwing examination of the available data, Acti e Region 2776 (Boulder SESC #) was selected for this particular illustration. We have presented a detailed discussion of this region in Section II of this report, and it will not be repeated here.

Some observed parameters related to a "shear index" for the interval 3-5 November 1980 are summarized in Table IV.1: shear angle, length of the involved neutral line, strength of the magnetic field, and magnitude of the magnetic field gradient. These parameters have been found to be related to the occurrence

of solar flares. For example, the shear angle and strength of the magnetic field at flares onset sites (along the "neutral line") have been quantitatively related to the occurrence of significant flares (Hagyard, 1984). The length of the sheard neutral line is related to the stored energy volume and the field strength is related to the energy available. The local magnetic field gradient may be related to the triggering mechanism, since the magnetohydrodynamic (MHD) instability is related to the local magnetic field gradient.

TABLE IV.1

2776 SHEAR PARAMETERS

Nov. 1980	Shear Angle	Neutral Line Length (km)	Transveral ß Field $ß_r$ (Gauss)	Magnetic Field Gradient (Gauss/km) Northeast	West
3rd	70-80°	~<8000	1100	increase	
4th	70-80°	~<10,000	1300	to	~0.11
5th	88°	~<20,000	1500	0.35	~0.23

As shown in Table IV.1, the observed shear angle (the difference between the observed transverse magnetic field orientation and the calculated potential field orientation) is ~70-80^0 on November 3rd and 4th. This increased to ~88^0 on the 5th, the day the first large flare was observed along thia neutral line. This relationship has also appeared in our numerical simulation results. For instance, the evolution of the magnetic field configuration resulting from the simulation of the magnetic field configuration resulting from the simulation model,

as shown in Figures III.3, III.6, and III.9, indicates in all these cases that the magnetic fielld evolves in an orderly manner in the initial stage (~100 Alfvenic time). However, when it reaches some critical time, the field configuration will change drastically in a very short time scale (i.e., one Alfvenic time). Physically, this can be understood by the analogy of a tensile test of engineering materials. This test shows that when we apply a force to stretch a wire, the stress and strain behavior is linear, as is stated in Hook's law, until it reaches the yielding point stage. At this point the stress and strain relationship will become quite irregular, with rapidly increasing strain with out increasing stress, then the rod breaks. This can be seen similary in the case of a solar flare. As we have observed from our simulation results, the largest amount of energy increase is when the inital field strength has the highest value (i.e., small $\beta_0{}^0$). The largest energy dissipation is where the resistivity is the largest. One way to increase the value of resistivity is by increasing the local magnetic field gradient. All these ingredients can be inferred from the observed values.

The 3-5 November 1980 interval, as summarized observationally in Table IV.1. As discussed above, the shear angle is seen to have increased from ~70^0 on 4 November to ~88^0 on 5 November. For the same interval, the length of the highly sheared portion of the neutral line also increased , from ~8000 km to ~20,000 km, a factor of 2.5. This length increase implies that the volume which contained the available magnetic energy, and (along with the shear angle increase) that the total

available energy increased significantly. Also, the observed data show an increase of local longitudinal magnetic field gradient across both the notheastern (the most sheared area) and the western sections of the evaluted neutral line. Based on these observed values, we immediately eliminated simulation Case III from further consideration, because the shear angle at the neutral line never reached the observed values of ~88^0. From Table III.2, we can find the most favorable energy dissipation rate for the two remaining cases:

CASE I yields an energy dissipation rate of 7.8×10^{14} erg/km^3s. The volume was estimated from the length of the neutral line, which is 2×10^4 km, as $(2 \times 10^4)^3$. thus the amount of energy which could be released within this volume is 6.24×10^{27} erg/s. A typical flare, lasting about 20 minutes, gives ~7.5×10^{30} ergs.

Case II gives an energy disipation rate of 8.9×10^{13} ergs/km^3 s, with the same conditions described in CASE I, leading to a toatal possible energy release of 8.5×10^{29} ergs.

In our comparison of these two cases, we find that CASE I is more favorable than the other simulation cases presented in this study.

In summary, we have presented a method for intercommecting the observations and the simulation model. By utilizing the model, we can estimate the amount of energy available for release form a sheared area within an active region. Furthermore, the model can also give the most likely location of the energy release. Again, we must emphasize that

this is a preliminary investigation. Before using the model as a prediction tool, more extensive investigation of this kind is required, until a satisfactory statistical confidence level can be established.

V. Concluding Remarks

In this final report, we have discussed the work performed under the contract AFGL (F19628-83-K-0019) during the period from November 12, 1982 to September 30, 1985. The achievements can be summarized as follows:

1. Data Analysis

Active Regions, selected on the basis of their size and strength (appearing at least potentially capable of producing significant flaring activity) and the availability of the appropriate data, were analyzed for observational evidence of storage of "available" magnetic energy (available for rapid release as solar "events"). Promising magnetic field parameters selected for analysis and correlation with flare production (location/level of activity) were 1) the angle of shear, defined as the angular difference between the calculated (or estimated) orientation of the potential field transverse component and the actual orientation (determined from observations) of the transverse component, 2) the strength of the magnetic field in the most strongly affected volume, 3) a parameter (length of included longitudinal neutral line) related to the affected volume, 4) dBL/ds, the gradient in the longitudinal component of the magnetic field (determined from any calibrated and spatially resolved longitudinal magnetogram), and in selected cases, 5) the

calculated vertical component of the electric field and 6) the calculated and projected magnetic energy buildup, based on photospheric proper motions, as determined from sunspot observations (MHD modeling).

Data considered necessary to the analysis were 1) vector magnetograms of the active region (single source - Marshall Space Flight Center Solar Observatory), 2) for correlation with energy storage parameters, dependably consistent, high quality flare observations (primarily AWS/SOON optical observations, and NOAA GOES x-ray flare data, both dependably available via the NOAA/AWS solar network), and 3) Hydrogen Alpha filtergrams, preferably AWS/SOON obtained high-resolution region H-alpha, used to determine the location of flare onset and flare kernels, and for comparison/correlation of (implied) chromospheric and photospheric magnetic structure.

For several active regions producing large and/or frequent flares, and with several counter-examples where there were no significant flare occurrences, we found that the flares clearly preferentially occurred in areas where observational evidence of significant shear was present. By application of the MHD model (Wu et al. 1983), using the observed photospheric shearing motion, it has also been demonstrated that the magnetic shear can supply enough energy for flare production. In cases (three) where data have permitted adequate analysis, it is also convincingly shown that the maximum shear angle is related to the location of frequent and/or large flares. Conversely, areas otherwise impressive (i.e. large sunspot groups with strong

magnetic fields) have been observed to be far less productive of flares. Initial steps have been taken toward the formulation of a "shear index", as a predictor of the location and level of solar activity. Testing and any appropriate modification of the initial, tentative index is expected to be possible in the increased activity in the new solar cycle.

2. MHD Modeling

A two dimensional, non-planar, time-dependent magnetohydrodydnamic (MHD) model, with and without joule dissipation, has been developed for the study of flare energy buildup and release and their relationship to observed flare prediction parameters. We have utilized observed and theoretical parameters as model inputs, and examined the model output in qualitative comparison with observed results. The model output physical parameters are; magnetic energy density, total energy, thermal dynamic properties of the solar plasma (i.e. density ρ, temperature T, and velocity field). Based on these computed physical parameters, we have demonstrated that shearing motion (a shearing index) is a good candidate for flare prediction, since the magnetic energy generated by shear motion is shown to provide more than adequate flare energy. The model also shows this energy to be concentrated in a localized region (Wu et al., 1984), which gives clear indication of the MHD instability developing for possible flare triggering. We have not yet completely integrated the observations and the MHD model, and there have been a very limited number of regions lending themselves to this composite analysis/modeling (due to solar cycle near minimum, and

intermittent observatory equipment upgrading. Some further develoment in this direction is needed.

REFERENCES

1. Calquist, P., Cosmic Electrodynamics, 3, 377, 1972.

2. de Loach, A. C., Hagyard, M. J., Rabin, D. M., Moore, R. L., Smith, J. B., Jr., West, E. A., and Tandberg-Hanssen, E., "Photospheric Electric Current and Transition Region Brightness Distributions", Solar Physics, --, (1984).

3. Hagyard, M. J.,"The Relation of Sheared Magnetic Fields to the Occurrence of Flares", Proceedings of the Workshop on Solar-Terrestrial Predictions, Meudon, France June 18-22, 1984, Artificial Satellites, 1986.

4. Hagyard, M. J., Smith, J. B. Jr., Tueber, D., and West, E. A., "A Quantitative Study Relating Observed Shear in Photospheric Magnetic Fields to Repeated Flaring", Solar Physics, 91(1), 115-126, 1984

5. Krall, K. R., Smith, J. B., Jr., Hagyard, M. J., West, E. A. and Cumings, N.P., "Vector Magnetic Field Evolution and Associated Photospheric Velocity Shear Within a Flare-Productive Active Region", Solar Physics 79, 59, 1982.

6. Smith, J. B. Jr. and Hagyard, M. J., "The Correlation of Flare Occurrence with the Observation of Magnetic Shear", presented at the SMA Symposium, 25th Plenary Meeting of COSPAR, Graz, Austria, 1984.

7. Svestka, Z., Solar Flares, Reidel Publishing, 1976

8. Van Hoven, G., in E. R.Priest (ed.) Solar Flare Magnetohydrodynamics, Gordon and Breach, London, Chapter 4, 1981.

9. Van Hoven, G, et al., Solar Flares (Peter A. Sturrock, ed.) Colorado Associated University Press, 1980.

10. West, E. A. and Hagyard, M. J., "Interpretation of Vector Magnetograph Data Including Magneto-Optics Effects", Solar Physics 88, 51, 1983.

11. Wu, S. T., Y, Q. Hu., Y. Nakagawa and E. Tandberg-Hanssen, "Induced Mass and Wave Motions in the Lower Solar Atmosphere I. Effects of Shear Motion of Flux Tubes, The Astrophysical Journal, 266, 866-881, 1983.

12. Wu, S. T., Y. Q. Hu, K. R. Krall, M. J. Hagyard, and J. B. Smith, Jr., "Modeling of Energy Buildup for a Flare-Productive Region" Solar Physics 90, 117-131, 1984.

13. Wu, S. T., Y. Q. Hu, Y. Nakagawa, and E. Tandberg-Hanssen, "Induced Mass and Wave Motions in the Lower Solar Atmosphere. II. Effects of Converging and Diverging Photospheric Motions, The Astrophysical Journal, 306, 751- 761, 1986.

14. Wu, S. T., J. J. Bao, Y. C. Xiao and J. B. Smith, Jr., "Fields, Currents, and Plasma Properties in a Solar Active Region Due to Photospheric Shear", Proceedings of the Solar Terrestrial Prediction Workshop, Paris, France, June 1984.

15. Wu, S. T., J. J. Bao and J. F. Wang, "Numerical Simulation of Flare Energy Buildup and Release via Joule Dissipation", Journal of Advance Space Research, Pergamon Press, 1987.

APPENDIX

PUBLICATIONS AND PRESENTATIONS

RESULTING FROM THIS RESEARCH PROGRAM

Modeling of Energy Buildup for a Flare Productive Region, by S. T. Wu, Y. Q. Hu, K. R. Krall, M. J. Hagyard, and J. B. Smith, Jr., Solar Physics, 90, 117-131, 1984.

The Correlation of Flare Occurrence with the Observation of Magnetic Shear, by J. B. Smith, Jr. and M. J. Hagyard, presented at the SMA Symposium, 25th Plenary Meeting of COSPAR, Graz,Austria, June 25-27, 1984.

A Quantitative Study Relating Observed Shear in Photospheric Magnetic Fields to Repeated Flaring, M. J. Hagyard, J. B. Smith, Jr., D. Teuber, and E. A. West, Solar Physics, 91, (1), 115-126, 1984.

Photospheric Electric Current and Transition Region Brightness Within an Active Region, by A.C. deLoach, M. J. Hagyard, D. Rabin, R.L. Moore, J. B. Smith, Jr., E. A. West, and E. Tandberg-Hanssen, Solar Physics, 91 (2), 235-242, 1984.

A Multiwave Study of a Double Impulsive Flare by K. T. Strong, A.O. Benz, B. R. Dennis, J.W. Leibacher, R. Mewe, A.I. Poland, J. Schrijver, G. Simnett, J. B. Smith, Jr., and J. Sylvester, Solar Physics, 91, 2, 325-344, 1984.

Electric Currents in Active Regions by M.J. Hagyard, E. A. West and J. B. Smith,Jr., to appear in Proceedings, Kunming Workshop on Solar Physics and Interplanetary Travelling Phenomena, (workshop in Yunnan Observatory, Kunming, People's Republic of China, November 1983), (1984).

Homologous Flares and the Evolution of NOAA Active Region 2372, K. T. Strong, J. B. Smith, Jr., M. McCabe, M.Machado, J. L.R. Saba, and G. M. Simnett, to appear in Advances in Space Research, Proceedings of the 25th Plenary Meeting of COSPAR, Graz, Austria, 1984.

The Solar/Interplanetary/Magnetosphere/Ionosphere Connection: A stretegy for Prediction of Geomagnetic Storms by M. Dryer, S.-I. Akasofu, H. W. Kroehl, R. Sagalyn, S. T. Wu, T. F. Tascione, and Y. Kamide, in Proceedings of AAS/AIAA Astrodynamics Specialist Conference, Paper AAS-85-313, 1985.

MHD Analysis of the Evolution of Solar Magnetic Fields and Currents in an Active Region by S. T. Wu, J. W. Wang, and E. Tandberg-Hanssen, in Unstable Current Systems and Plamsa Instabilities in Astrophysics, International Astronomical Union Symposium #107, Vol. 1, 487-490, 1985.

A Multiple Type II Burst Associated with a Coronal Transient and Its MHD Simulation by T. E. Gergely, M. R. Kundu, S. T. Wu, M. Dryer, Z. Smith, and R. T. Stewart, in "Advances in Space Reserach - Solar Maximum Analysis", Pergamon Press, Vol. 4, Issue 7, 283-286, 1984.

On the Heating Mechanism of Magnetic Flux Loops in the Solar Atmosphere by M. T. Song and S. T. Wu, "Advances in Space Research - Solar Maximum Analyses" Pergamon Press, Vol. 4, Issue 7, 275-278, 1985.

Computer-Simulated Active Solar Phenomena by S. T. Wu, Conference Paper, presented at Kunming International Workshop on Solar Physics and International Travelling Phenomena, Nov. 21-15, 1983.

Numerically-Simulated Formation and Propagation of Interplanetary Shocks by S. T. Wu in "Computer Simulation of Space Plasmas", D. Reidel Publishing Co., 179-201, 1984

On the Numerical Computational of Nonlinear Force-Free Magnetic Fields by S. T. Wu, H. M. Chang and M. J. Hagyard, in NASA Conference Publication 2374 "Measurements of Solar Vector Magnetic Fields" 17-48, 1985.

Induced Mass and Wave Motions in the Lower Solar Atmosphere. II. Effects of Converging and Diverging and Photospheric Motions, by S. T. Wu, Y. Q. Hu, and Y. Nakagawa, and E. Tandberg-Hanssen, Astrophysical Journal, 306, 751-761, 1986

Magnetohydrodynamics (MHD) Modelling of Flare Energy Buildup, The Energy Release Phase, and Its Propagation into Heliospheric Space, by S. T. Wu and S. Panitchob in Proceedings of the SMA 1986.

The Correlation of Flare Occurence with the Observation of Magnetic Shear by J. B. Smith, Jr. and M. J. Hagyard presented at the SMA Symposium, 25th Plenary Meeting of COSPAR, Graz, Austria, June 25 - July 7, 1984.

A Quantitative Study Relating Observed Shear in Photospheric Magnetic Fields to Repeated Flaring by M. J. Hagyard, J. B. Smith, Jr., D. Teuber and E. A. West, Solar Physics, 91(1), 115-126, March 1984.

Electric Currents in Active Regions by M. J. Hagyard, E. A. West and J. B. Smith, Jr. to appearin Proceedings, Kunming Workshop on Solar Physics and Interplanetary Travelling Phenomena, (workshop in Yunnan Observatory, Kunming, People's Republic of China, November 1983) (1984).

Homologous Flares and the Evolution of NOAA Active Region 2372, by K. T. Strong, J. B. Smith, Jr., M.McCabe, M. Machado, J.L. R. Saba and G. M. Simnett, to appear in Advances in Space Research, Proceedings of the 25th Plenary Meeting of COSPAR, Graz, Austria, 1984